Structural Basis for Substrate-Dependent Allostery in Oxygen Activation by a Cytochrome P450 Enzyme Revealed by Analysis at Different Temperatures

Matthew N. Podgorski,[a],¶ Daniel P. McDougal,[b], ¶ Eleanor C. Campbell,[c], John B. Bruning,[c], and Stephen G. Bell*[a]

[a] Department of Chemistry, University Adelaide, Adelaide, SA, 5005, Australia

* Corresponding author: E-mail; stephen.bell@adelaide.edu.au

[b] School of Biological Sciences, University of Adelaide, Adelaide, SA, 5005, Australia

[c] Australian Synchrotron, 800 Blackburn Rd, Clayton, Melbourne, VIC, 3168. Australia

¶ These authors contributed equally

Supporting Information

Supporting Information

CYP Catalytic Cycle

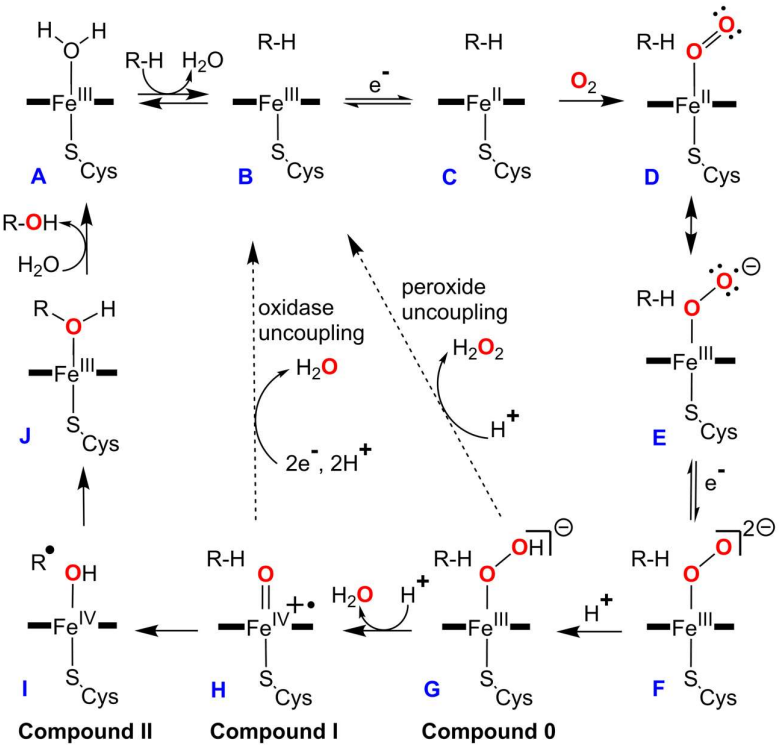

Scheme S1. The cytochrome P450 catalytic cycle including the peroxide and oxidase uncoupling pathways.

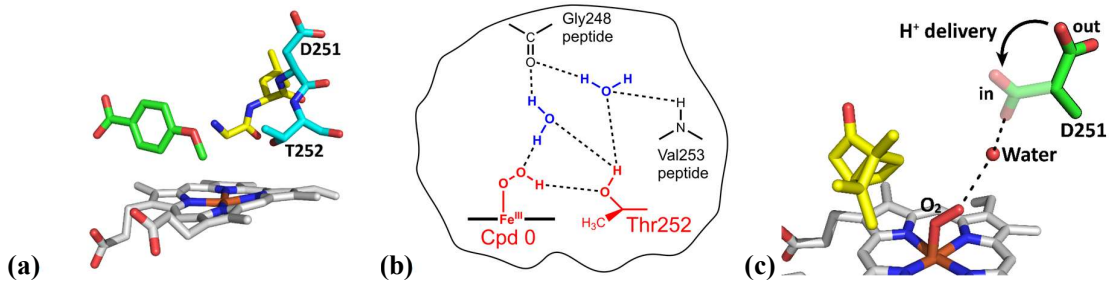

Figure S1. Two protons are required to convert the ferric-peroxo anion into Cpd I. **(a)** Proton delivery is facilitated by a highly conserved acid-alcohol pair of residues (usually threonine and aspartate). In CYP199A4, the acid-alcohol pair is D251 and T252.[1] **(b)** The threonine (T252) residue forms a hydrogen-bond with the ferric-hydroperoxy intermediate (Cpd 0), stabilising Cpd 0 and increasing its proton affinity which aids the subsequent protonation step.[2] **(c)** The aspartate residue (D251), of $P450_{cam}$ has a crucial role in proton delivery.[2] In most X-ray crystal structures the aspartate residue is located outside of the active site, and it would need to rotate into the active site during the catalytic cycle to deliver the protons. The necessary rotation of D251 is described by the black arrow.[3]

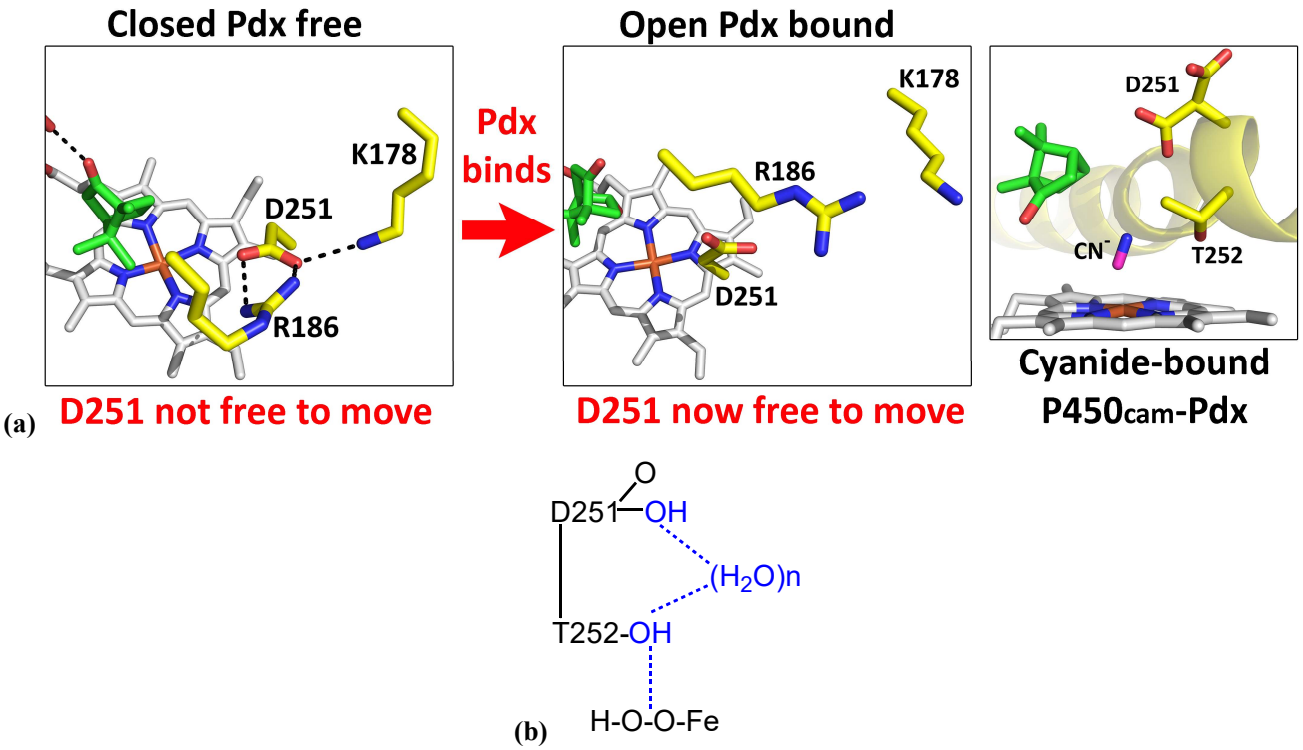

Figure S2. (a) $P450_{cam}$ (CYP101A1) is the most extensively studied P450. In $P450_{cam}$, D251 is *not* able to move into the active site as it is immobilised by strong interactions with Lys178 and Arg186 (PDB entry: 2CPP).[4] A complicated theory has been proposed that the enzyme opens when the ferredoxin (Pdx) binds, breaking these salt bridges and then allowing D251 to move (PDB entry: 4JX1).[4] In the cyanide-bound form of the $P450_{cam}$-Pdx complex (shown here), D251 was observed to rotate into the active site (PDB entry: 6NBL).[5] **(b)** It was suggested by Ugur *et al.* that D251 delivers protons to the active site via the pathway depicted here.[6]

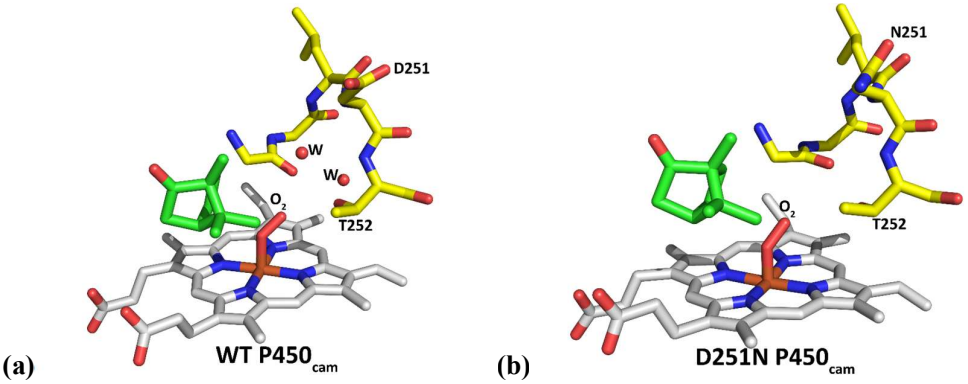

Figure S3. The crystal structures of O_2-bound ferrous WT and D251N $P450_{cam}$ demonstrated that the D→N mutation distorted the active-site structure so that two key water molecules are absent in the D251N structure.[2] The hypothesis put forward by Nagano *et al.* is that the D251 residue has no role in proton delivery, but the two water molecules that are omitted in the D251N mutant are important.[2]

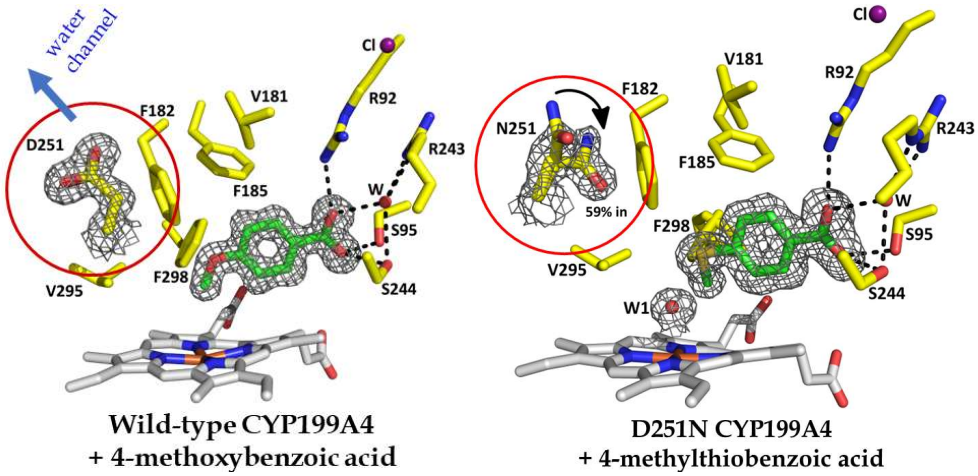

Figure S4. Left: In wild-type CYP199A4, the aspartate (D251) is located outside of active site and points into a water channel. Shown here is a 1.26-Å crystal structure of WT CYP199A4 bound to 4-methoxybenzoic acid at 100 K (PDB code: 9DOE. **Right:** Certain crystal structures at 100 K of the D251N mutant of CYP199A4 (in which aspartate 251 had been mutated to an asparagine) showed that the mutated residue had rotated into the active site. The crystal structure shown here is the 1.44-Å structure of the D251N mutant bound to 4-methylthiobenzoic acid (PDB code: 7TQM), in which the N251 side chain has partially rotated into the active site (59% occupancy). The $2mF_o$-DF_c composite omit map of the substrate and residue 251 is shown as grey mesh (contoured at 1.0 σ or 1.5 σ).

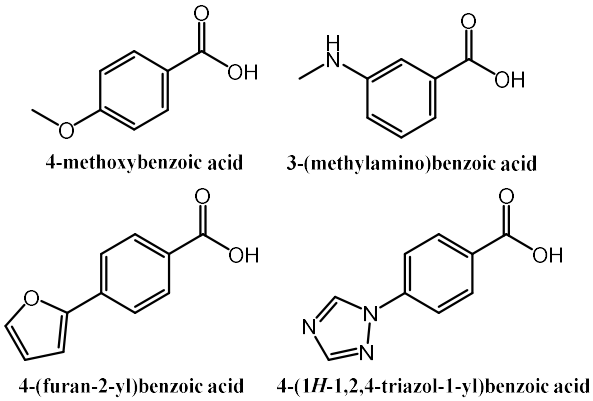

Figure S5. Substrates and ligands crystallised with CYP199A4 in this (top) and other studies (bottom) (PDB codes: 4DO1, 6PRR, 7TRT, and 7N14).[7-10]

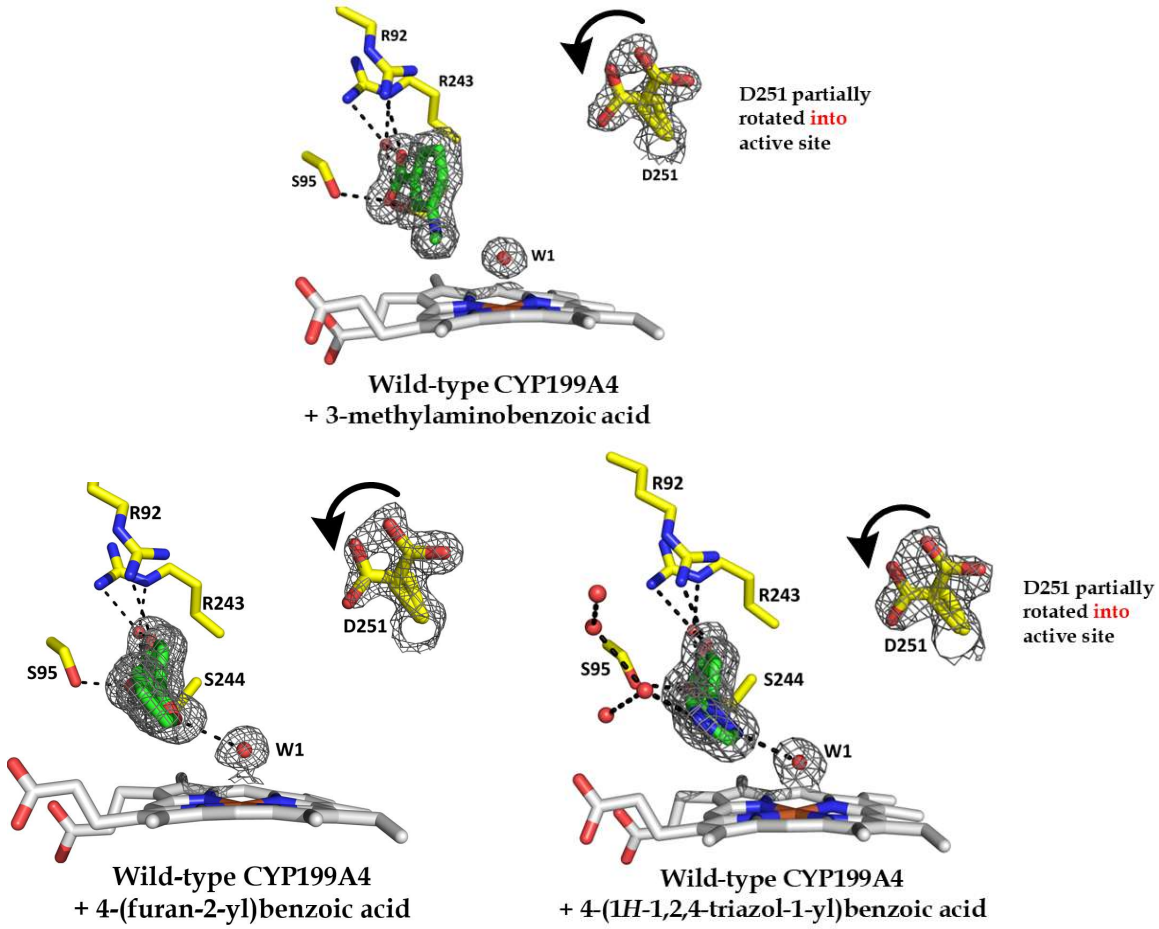

Figure S6. Crystal structures of wild-type CYP199A4 at 100 K with certain ligands bound showed that D251 had partially rotated into the active site.[7-9] For example, in the 100 K crystal structures of WT CYP199A4 bound to 3-methylaminobenzoic acid[9] (**top; PDB code: 9MIM and 6PRR**, 4-furan-2-ylbenzoic acid[7] (**bottom left; PDB code: 7TRT**) and 4-(1*H*-1,2,4-triazol-1-yl)benzoic acid[8] (**bottom right; PDB code: 7N14**), D251 is present in two conformations. In one conformation, the side chain points out into the water channel, and in the other, the side chain has rotated into the active site. The $2mF_o$-DF_c composite omit map of the substrate, heme-bound aqua ligand and D251 side chain is shown as grey mesh (contoured at 0.7 or 1.0 σ).

Table S1. Crystallographic data table for the crystal structures of CYP199A4 in complex with 3-methylaminobenzoic acid at 100, 150 and 200 K. The space group is $P12_11$.

	The crystal structure of CYP199A4 bound to 3-methylaminobenzoic acid		
	Dataset 1: 100 K	**Dataset 2: 150 K**	**Dataset 3: 200 K**
PDB code	**9MIM**	**9MIO**	**9MJE**
Wavelength (Å)	0.95372	0.95372	0.95372
a/b/c (Å)	44.44/51.45/79.39	44.52/51.54/79.49	44.67/51.70/79.70
α/β/γ (˚)	90.00/92.20/90.00	90.00/92.19/90.00	90.00/92.19/90.00
Resolution (Å)	44.41-1.37 (1.39-1.37)	44.49-1.39 (1.42-1.39)	43.36-1.95 (2.00-1.95)
<I/σ(I)>	10.5 (1.3)	7.9 (1.0)	13.1 (6.3)
Unique reflections	75199 (3400)	71176 (2997)	26650 (1840)
Completeness	99.4 (89.5)	99.2 (85.4)	99.9 (99.9)
Redundancy	6.8 (6.7)	6.7 (6.5)	6.4 (6.6)
R_{merge} (%) (all I+ and I-)	9.0 (106.8)	13.1 (180.4)	13.6 (72.1)
R_{pim} (%) (all I+ and I-)	3.8 (44.0)	5.4 (74.3)	5.9 (30.1)
$CC_{1/2}$	99.9 (67.1)	99.7 (54.6)	99.0 (93.7)
R_{work} (%)	15.60	16.28	15.42
R_{free} (%)	16.74	18.33	19.02
r.m.s.d. bond lengths (Å)	0.004	0.004	0.004
r.m.s.d. bond angles (˚)	0.734	0.775	0.719
Ramachandran plot (%)			
Most favoured	98.47	98.21	98.21
Allowed	1.53	1.79	1.79
Outliers	0	0	0
Average B-factor (A^2)	16.67	17.37	22.17

Comparison of the new crystal structure of 3-methylaminobenzoic acid-bound CYP199A4 determined at 100 K to the previously solved structure

The structure of 3-methylaminobenzoic acid-bound CYP199A4 was previously determined at 100 K (PDB code: 6PRR). The resolution of this previously reported structure is 1.67 Å.

The new 100 K structure was determined at higher resolution (1.37-Å resolution) and is consistent with the previously determined structure.

In both structures, a high-occupancy heme-bound aqua ligand is present (~90% occupancy) and the D251 side chain has partially rotated into the active site (42 or 47% occupancy). The Fe-O and Fe-S bond lengths are similar in both structures; the Fe-O bond lengths are 2.20 and 2.26 Å, and the Fe-S bond lengths are 2.31 and 2.30 Å.

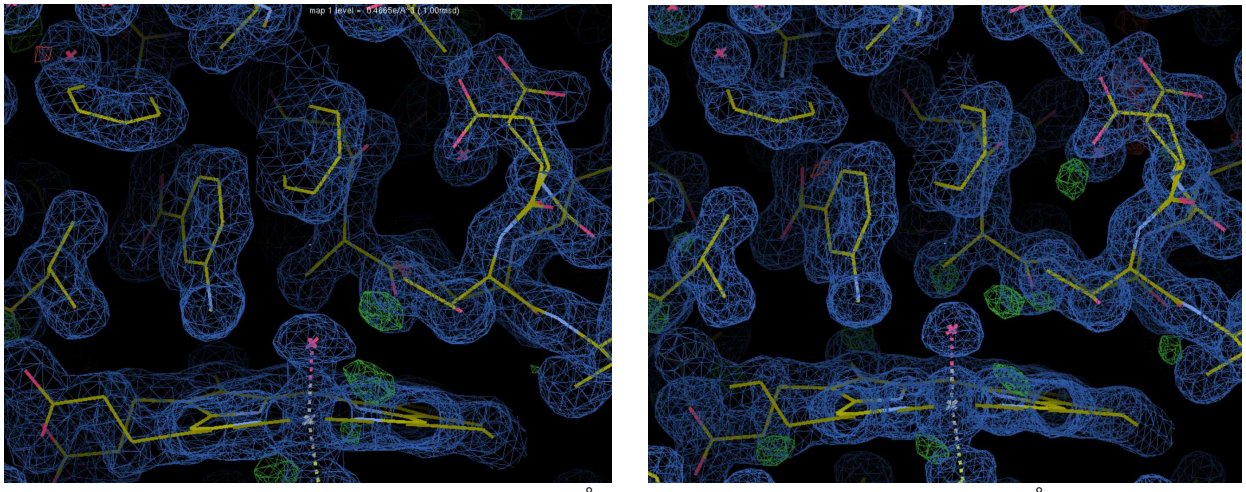

Previously solved structure (PDB code: 6PRR; 1.67-Å resolution) **New structure (1.37-Å resolution)**

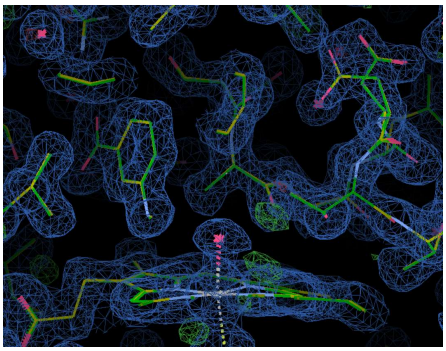

Above: Overlaying the new and previously determined structures (yellow and green sticks) demonstrates that the two structures are virtually identical.

Figure S7. Comparison of the new and previously solved structures of CYP199A4 bound to 3-methylaminobenzoic acid at 100 K.

Table S2. Table of occupancy data for the crystal structures of CYP199A4 bound to 3-methylaminobenzoic acid determined at 100 K

	Occupancy (%)	
	Previously solved structure (6PRR)	**New 100 K structure (9MIM)**
Heme-bound aqua ligand	90%	88%
Substrate	100%	100%
D251 conformation pointing into active site	42%	47%
D251 conformation pointing out of active site (into water channel)	58%	53%

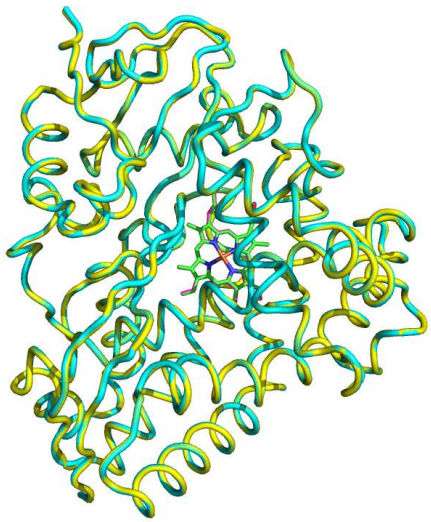

Figure S8. Overlaid Cα traces of the new and previously reported 100 K crystal structures of CYP199A4 bound to 3-methylaminobenzoic acid (PDB entries: 9MIM and 6PRR). The RMSD between Cα atoms is 0.057 Å (over all 393 pairs). The previously reported structure is depicted in cyan (with a green heme). The new structure is shown in yellow (with a magenta heme).

Dataset 1: The crystal structure of CYP199A4 bound to 3-methylaminobenzoic acid solved at 100 K

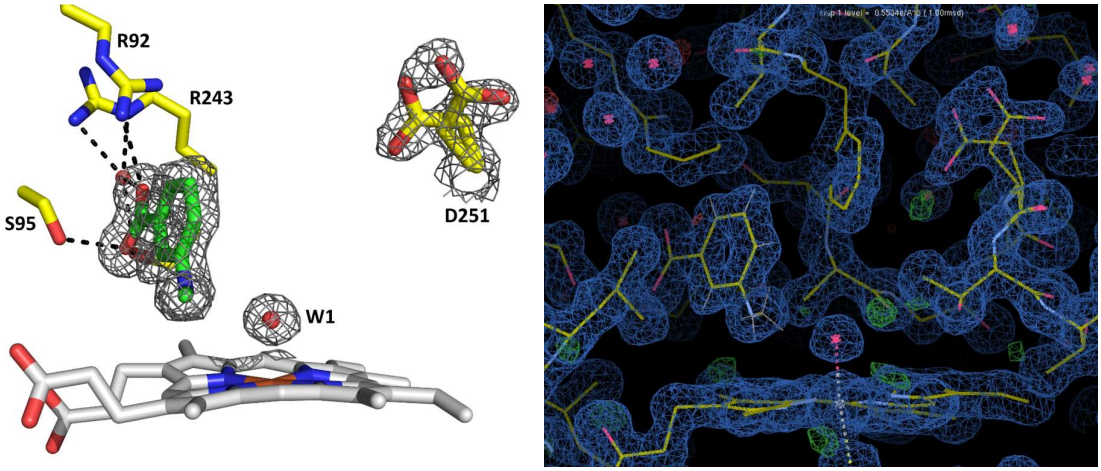

Figure S9. The crystal structure of CYP199A4 bound to 3-methylaminobenzoic acid solved at **100 K** (**1.37-Å** resolution). A *2mFo-DFc* composite omit map of the substrate, heme-bound aqua ligand (W1) and D251 side chain is shown as grey mesh contoured at 1.0 σ (1.5 Å carve).

Dataset 2: The crystal structure of CYP199A4 bound to 3-methylaminobenzoic acid solved at 150 K

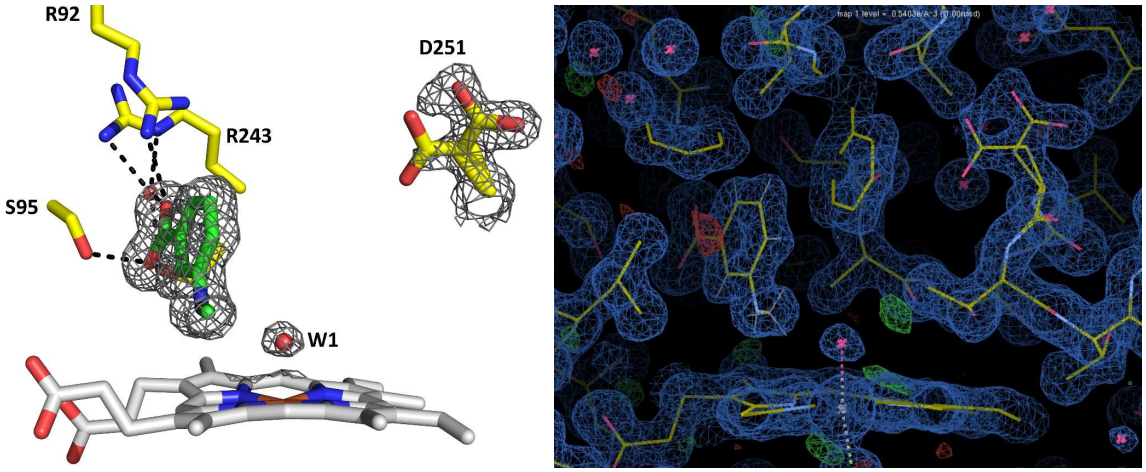

Figure S10. The crystal structure of CYP199A4 bound to 3-methylaminobenzoic acid solved at **150 K** (**1.39-Å** resolution). A *2mFo-DFc* composite omit map of the substrate, heme-bound aqua ligand (W1) and D251 side chain is shown as grey mesh contoured at 1.0 σ (1.5 Å carve).

Dataset 3: The crystal structure of CYP199A4 bound to 3-methylaminobenzoic acid solved at 200 K

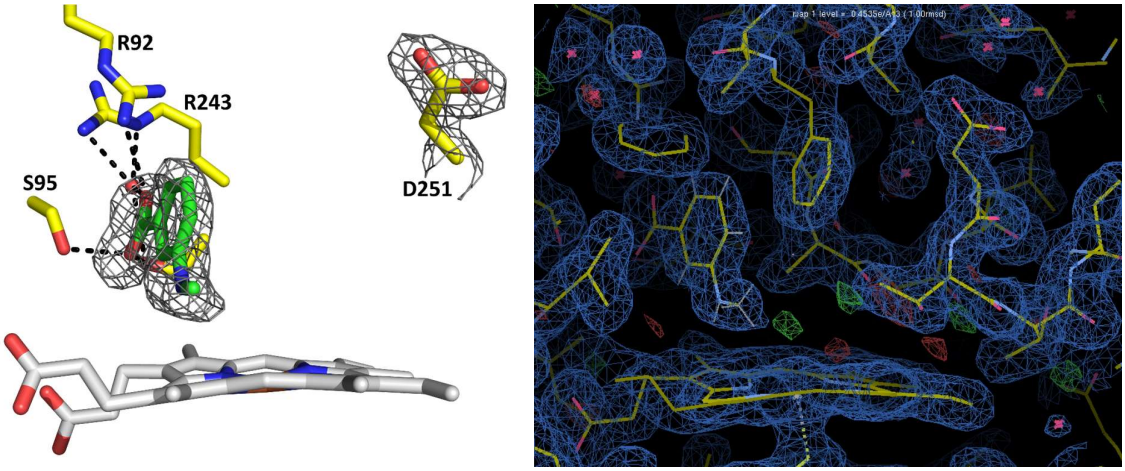

Figure S11. The crystal structure of CYP199A4 bound to 3-methylaminobenzoic acid solved at **200 K** (**1.95-Å** resolution). A *2mFo-DFc* composite omit map of the substrate and D251 side chain is shown as grey mesh contoured at 1.0 σ (1.5 Å carve). A heme-bound aqua ligand is not present in this structure.

Dataset 1: The crystal structure of CYP199A4 bound to 3-methylaminobenzoic acid solved at 100 K

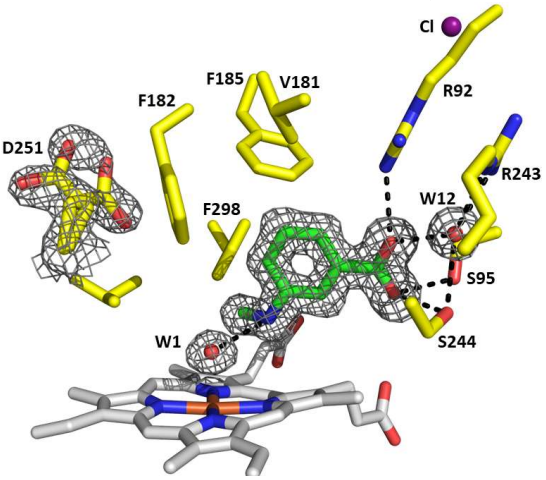

Figure S12. The crystal structure of CYP199A4 bound to 3-methylaminobenzoic acid solved at **100 K** (**1.37-Å** resolution). A *2mFo-DFc* composite omit map of the substrate, heme-bound aqua ligand (W1) and D251 side chain is shown as grey mesh contoured at 1.0 σ (1.5 Å carve).

Dataset 2: The crystal structure of CYP199A4 bound to 3-methylaminobenzoic acid solved at 150 K

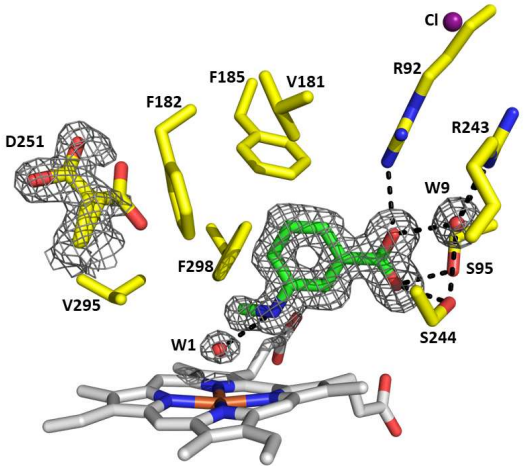

Figure S13. The crystal structure of CYP199A4 bound to 3-methylaminobenzoic acid solved at **150 K** (**1.39-Å** resolution). A *2mFo-DFc* composite omit map of the substrate, heme-bound aqua ligand (W1) and D251 side chain is shown as grey mesh contoured at 1.0 σ (1.5 Å carve).

Dataset 3: The crystal structure of CYP199A4 bound to 3-methylaminobenzoic acid solved at 200 K

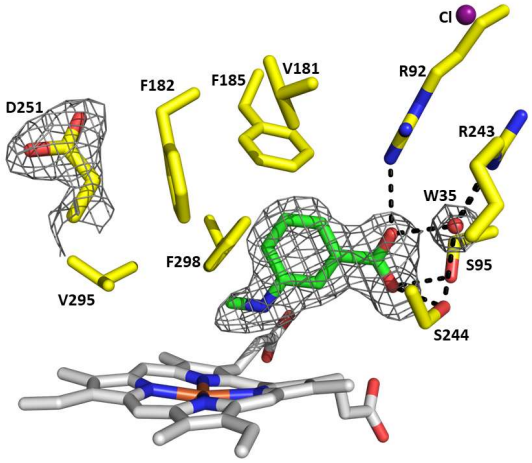

Figure S14. The crystal structure of CYP199A4 bound to 3-methylaminobenzoic acid solved at **200 K** (**1.95-Å** resolution). A *2mFo-DFc* composite omit map of the substrate and D251 side chain is shown as grey mesh contoured at 1.0 σ (1.5 Å carve). A heme-bound aqua ligand is not present in this structure.

Interactions of D251 with surrounding residues/water molecules

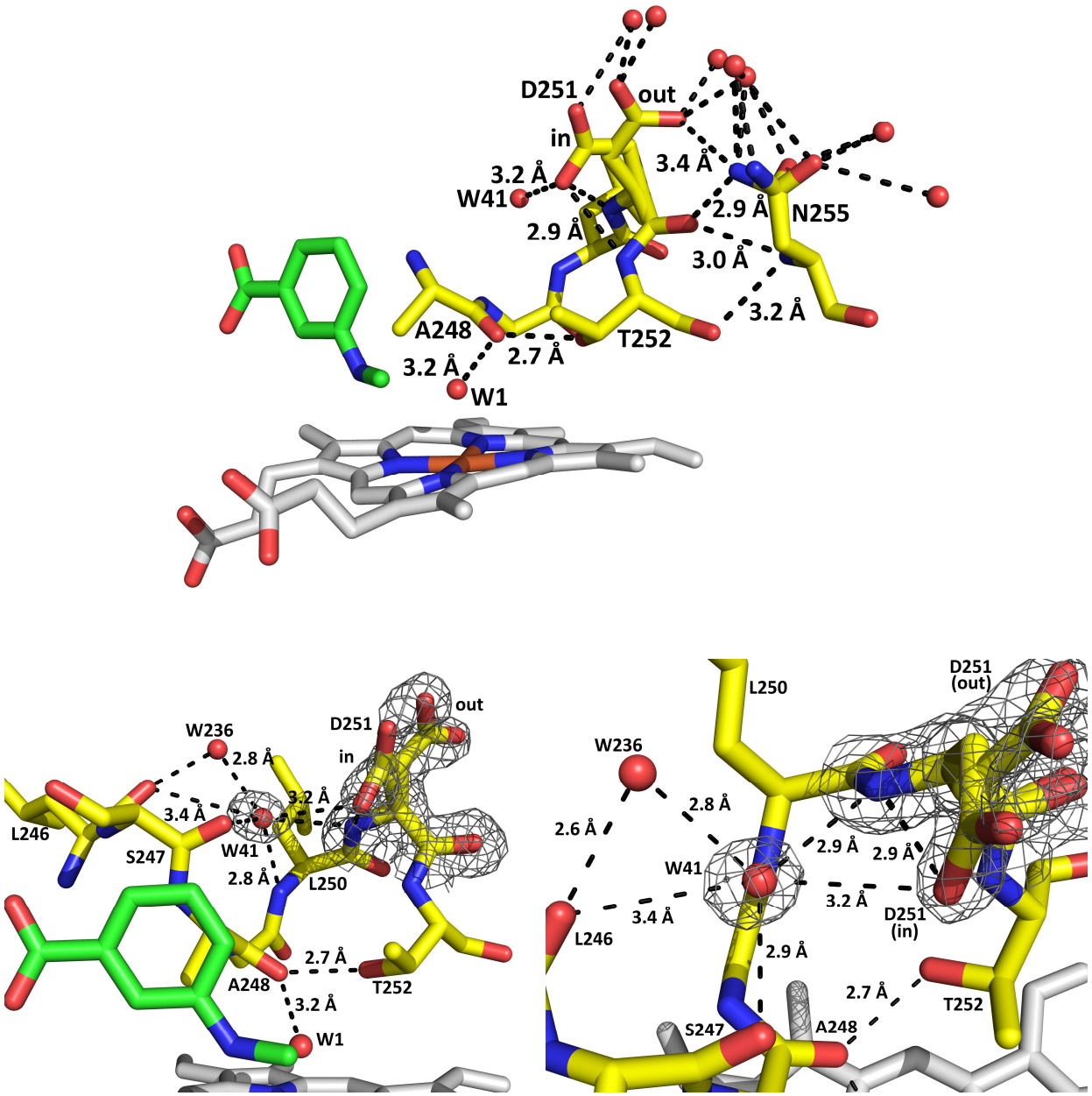

Figure S15a. The interactions of D251 with surrounding residues/water molecules in the crystal structure of WT CYP199A4 bound to 3-methylaminobenzoic acid at 100 K.

Polar interactions are represented by black dashed lines and were identified using PyMOL. When the D251 side chain rotates into the active site, there may be an interaction between the D251 carboxylate and W41 (3.2 Å).

There are also polar interactions between W41 and the NH of L250, the NH of D251, the carbonyls of S247 and L246, and W236.

See Figure S48 and S49 for information on the distances between selected atoms from these interactions in the MD simulations.

Space filling representation of the 'in' conformer of D251, showing van der Waals contacts to D251

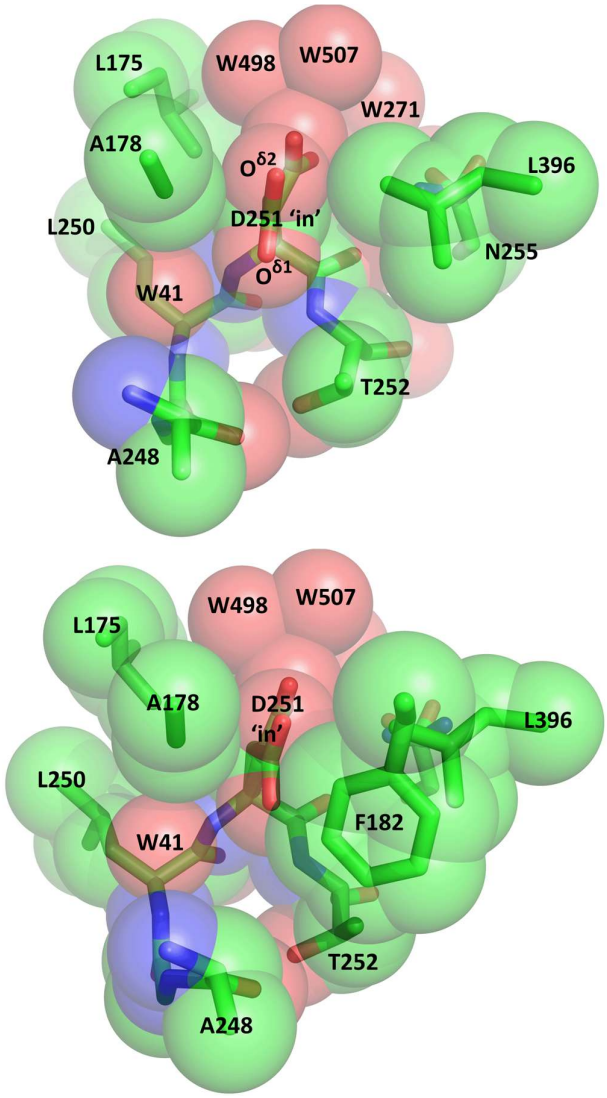

Figure 15b. A space filling representation of the D251 residue and surrounding residues/water molecules in the 100 K crystal structure of 3-methylaminobenzoic acid-bound CYP199A4. In the top figure, the F182 residue has been omitted for clarity.

W41 (located in the I-helix) interacts with multiple residues in the I-helix and a nearby water molecule. W41 is located approximately 9 Å away from the heme iron.

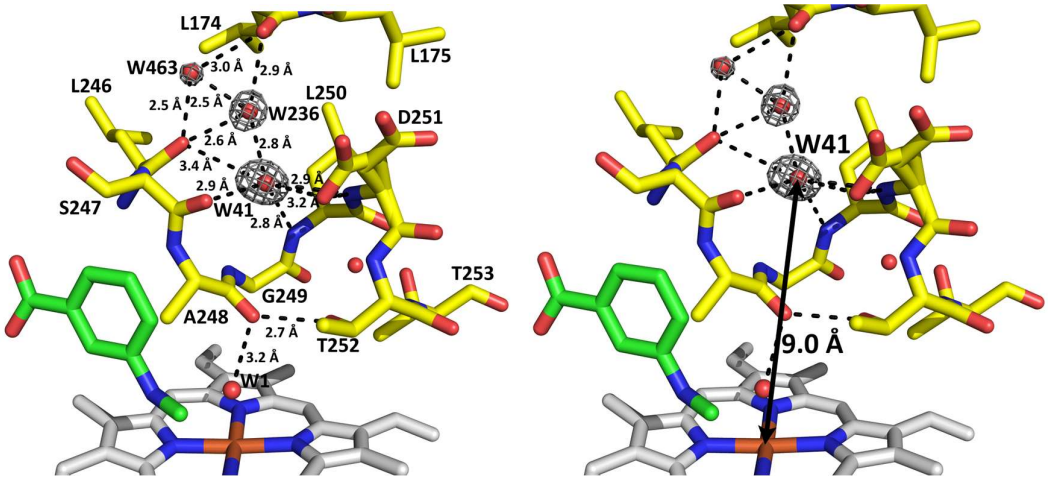

Figure S15c. The structure of the I-helix in the 100-K crystal structure of CYP199A4 bound to 3-methylaminobenzoic acid. W41 interacts with the D251 side chain carboxylate (3.2 Å), the backbone NH of L250 (2.8 Å), the backbone NH of D251 (2.9 Å), the backbone carbonyl of S247 (2.9 Å), the backbone carbonyl of L246 (3.4 Å) and a nearby water molecule (2.8 Å). These distances are labelled in the figure. A $2mF_o$-DF_c composite omit map of W41 and nearby water molecules is shown as grey mesh contoured at 1.0 σ.

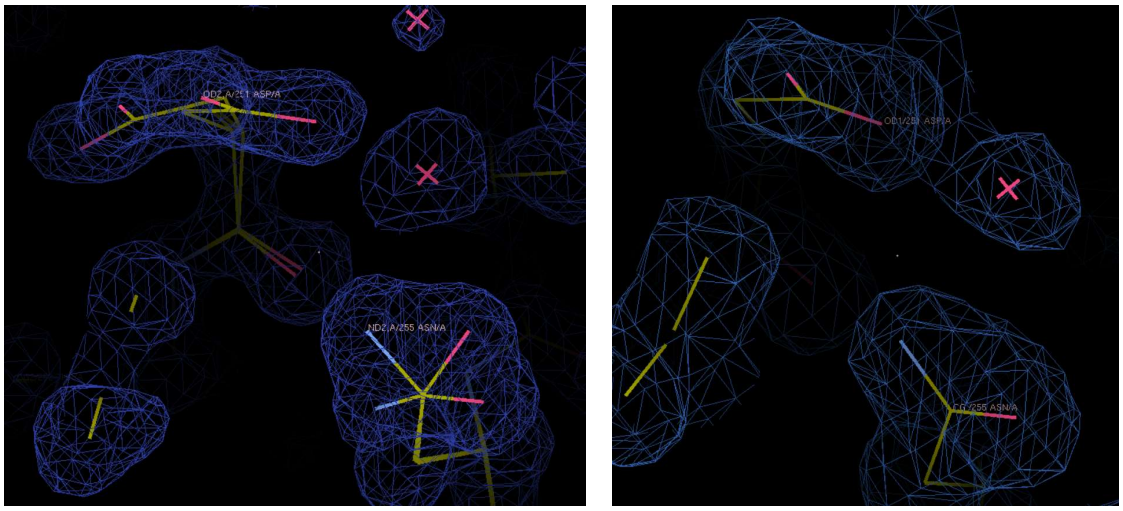

100 K **200 K**

Figure S15d. In the crystal structure of WT CYP199A4 bound to 3-methylaminobenzoic acid at 100 K, D251 has partially rotated into the active site, and it also appears that N255 has partially rotated. Shown above are the structures of WT CYP199A4 bound to 3-methylaminobenzoic acid at 100 K and 200 K. At 100 K, D251 is in two positions, and there are also two conformations of N255. At 200 K, D251 is only pointing out of the active site and there is only one conformation of N255.

Table S3. Position of the D251 side chain in the variable-temperature structures of CYP199A4 bound to 3-methylaminobenzoic acid

Dataset	Temperature	Occupancy of D251 conformation pointing into active site	Occupancy of D251 conformation pointing out of the active site (into the solvent channel)	Occupancy of N255 conformation H-bonded to D251	Occupancy of N255 conformation rotated by 90° away from D251	W41 occupancy*
1	**100 K**	47%	53%	64%	36%	89%
2	**150 K**	33%	67%	78%	22%	91%
3	**200 K**	Not present	100%	100%	Not present	84%

* The refined occupancy of the water molecule which interacts with D251 when it rotates into the active site (this water molecule is labelled W41 in the 100 K structure).

Table S4. Occupancy of the heme-bound aqua ligand (W1) in the variable-temperature structures of CYP199A4 bound to 3-methylaminobenzoic acid

Dataset	Temperature	Refined occupancy of the heme-bound aqua ligand
1	**100 K**	88%
2	**150 K**	45%
3	**200 K**	Not present

Overlaid crystal structures of CYP199A4 bound to 3-methylaminobenzoic acid at 100, 150 and 200 K

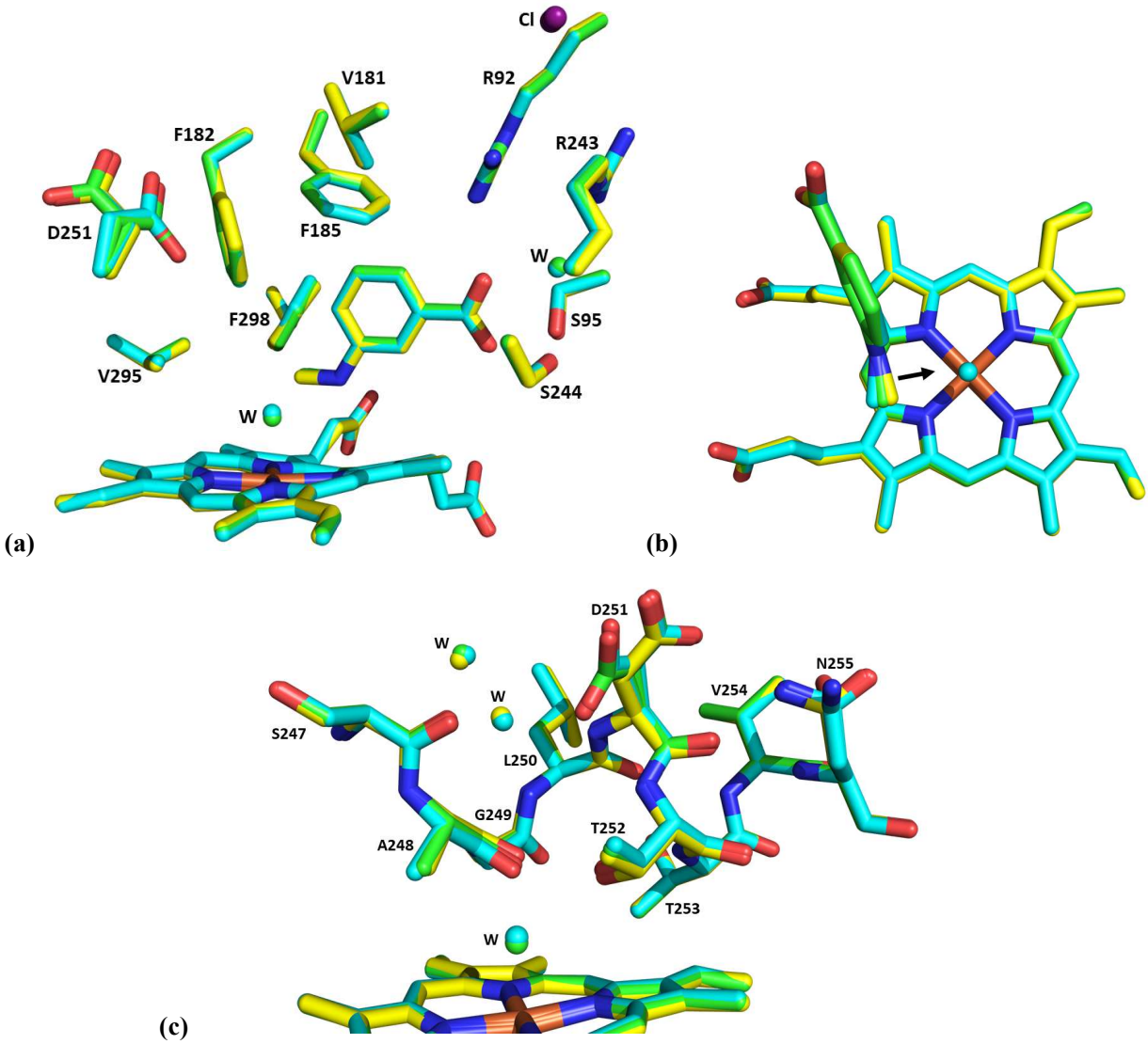

Figure S16. Overlaid crystal structures of CYP199A4 bound to 3-methylaminobenzoic acid at 100 K (blue), 150 K (green) and 200 K (yellow).

Movement of A248 in the variable-temperature crystal structures

Subtle movement of A248 occurred in certain CYP199A4 crystals when the temperature of the crystals was raised. In crystals where there is a high-occupancy heme-bound aqua ligand present at 100 K, the carbonyl of A248 has shifted closer to the heme. This may be due to a hydrogen bonding interaction between the A248 carbonyl and the heme-bound aqua ligand. As the temperature is raised and the heme-bound aqua ligand disappears (due to photoreduction of the heme), the carbonyl of A248 shifts further away from the heme. There is also subtle movement of the Cα atom of glycine 249 (by 0.4 Å).

Movement of A248 in the crystal structures of CYP199A4 bound to 3-methylaminobenzoic acid at 100, 150 and 200 K

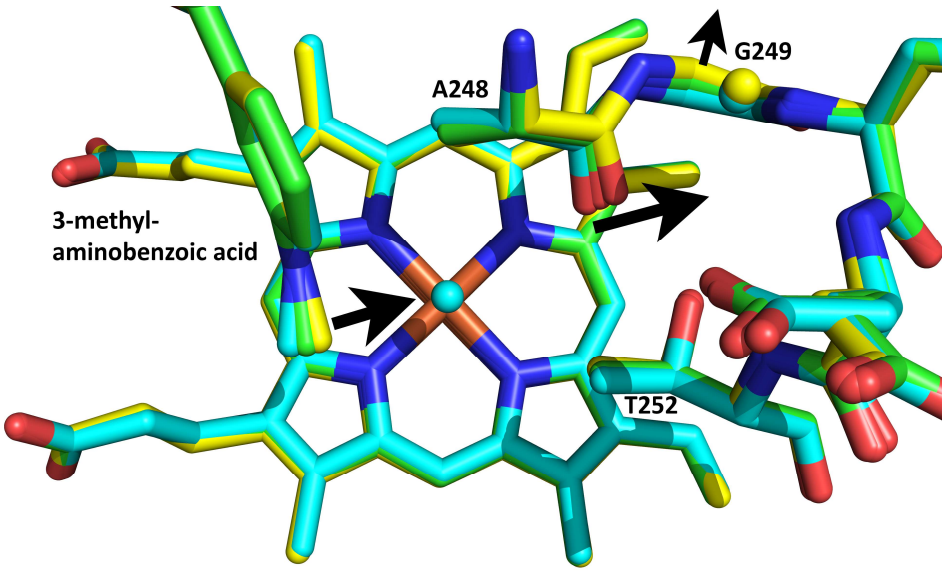

Figure S17. The overlaid crystal structures of CYP199A4 bound to 3-methylaminobenzoic acid at 100 K (cyan), 150 K (green) and 200 K (yellow). As the temperature is raised and the heme-bound aqua ligand disappears, the carbonyl of A248 shifts further away from the centre of the heme (movement described by the **black arrow**). The methylamino moiety of the substrate shifts closer to the centre of the heme as the heme-bound aqua ligand disappears (**black arrow**).

The methyl group of 3-methylaminobenzoic acid shifts by 0.5 Å, and the carbonyl oxygen of A248 shifts by 0.6 Å. The hydroxyl O of T252 shifts by only 0.3 Å. The Cα atom of G249 shifts by 0.4 Å (**black arrow**).

Displacement of the heme iron below the plane of the heme in the crystal structures of 3-methylaminobenzoic acid-bound CYP199A4

Table S5. Displacement of the heme iron below the plane of the heme in the crystal structures of 3-methylaminobenzoic acid-bound CYP199A4 (increasing temperature series)

Dataset	Temperature	Displacement of the iron below the heme plane*	Fe-S bond length
1	100 K	0.10 Å	2.30 Å
2	150 K	0.17 Å	2.37 Å
3	200 K	0.21 Å	2.35 Å

* plane defined by the four pyrrole nitrogens

Displacements were measured using UCSF Chimera.

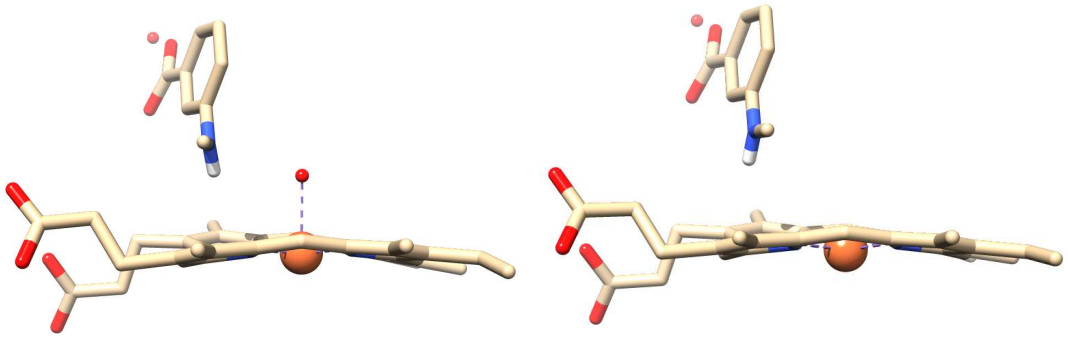

100 K **200 K**

Figure S18. Displacement of the heme iron below the plane of the heme in the crystal structures of 3-methylaminobenzoic acid-bound CYP199A4 at 100 K and 200 K.

Visual inspection of the electron density maps for radiation damage (e.g., decarboxylation of Asp/Glu side chains)

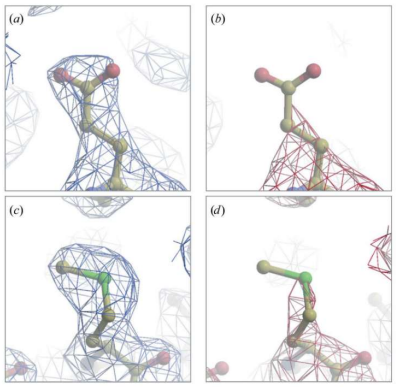

Figure S19. Aspartate, glutamate, tyrosine and methionine residues are susceptible to radiation damage.[11] Aspartate and glutamate residues are susceptible to decarboxylation, and methionine residues may undergo cleavage of the C-S bond.[11] Tyrosine residues also may lose the OH group. These forms of radiation damage are illustrated in the figure above[11]. This figure was reprinted with permission from the articles:
Garman, E. Radiation damage in macromolecular crystallography: what is it and why should we care? *Acta Cryst. D* **2010**, *66* (4), 339-351. DOI: 10.1107/S0907444910008656
Garman, E. F.; Owen, R. L. Cryocooling and radiation damage in macromolecular crystallography. *Acta Cryst. D* **2006**, *62* (1), 32-47. DOI: 10.1107/S0907444905034207

Table S6. Electron density maps of Asp/Glu residues in the three successive datasets at 100, 150 and 200 K.

The $2mF_o$-DF_c electron density map is shown contoured at 1.0 σ (blue mesh), and the mF_o-DF_c difference map is shown contoured at ± 3 σ (red and green mesh).

Residue	Dataset 1 100 K	Dataset 2 150 K	Dataset 3 200 K
Glu367	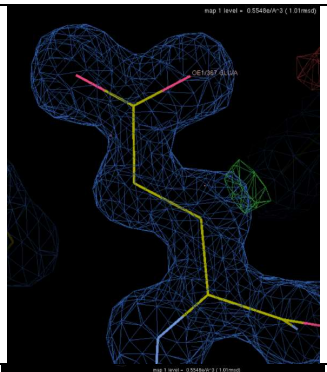	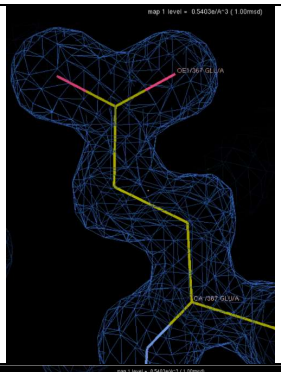	
Asp33		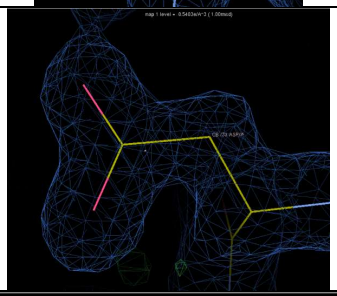	
Asp277	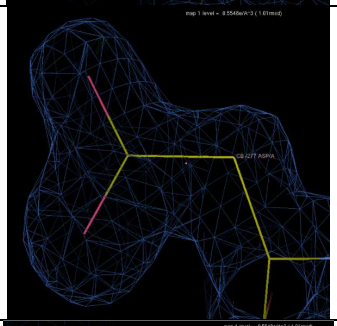	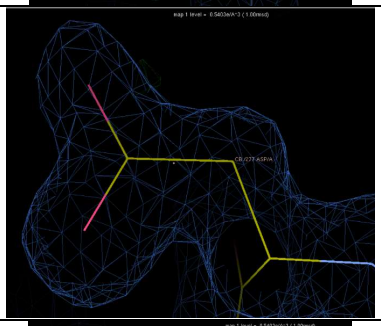	
Asp236		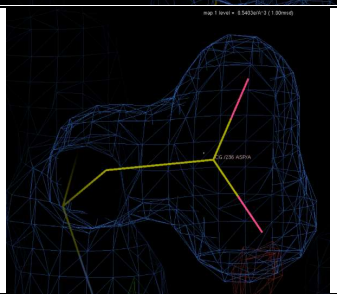	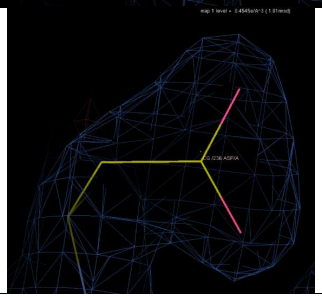

Asp70	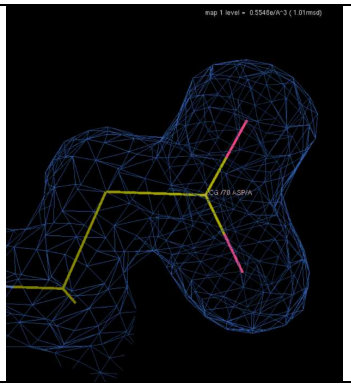	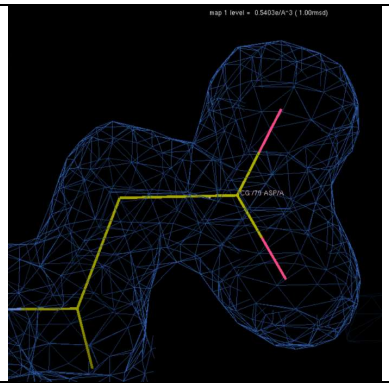	

Residue	**Dataset 1 100 K**	**Dataset 2 150 K**	**Dataset 3 200 K**
Glu63	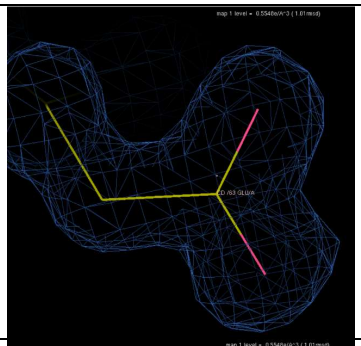	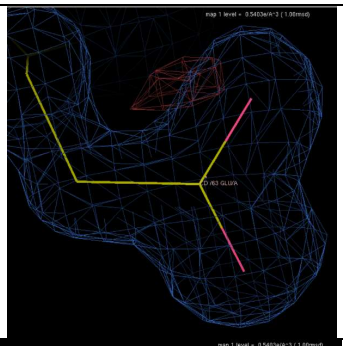	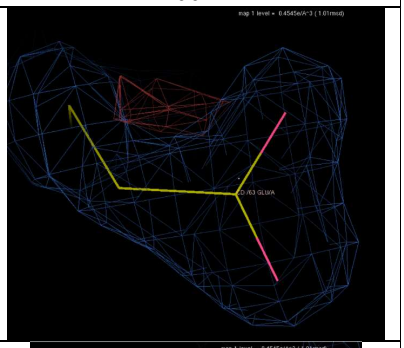
Asp329	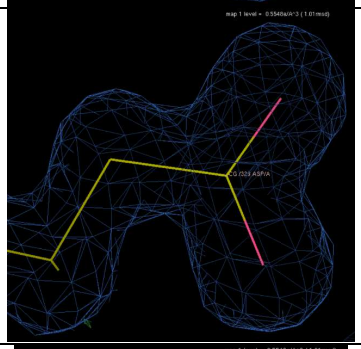	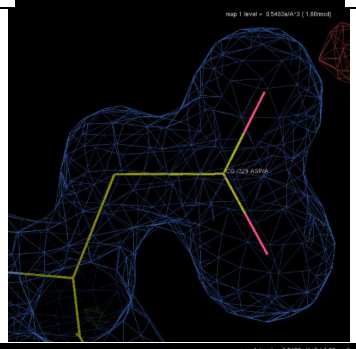	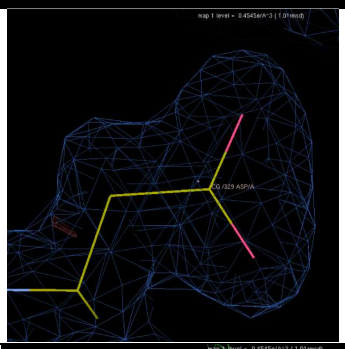
Glu305	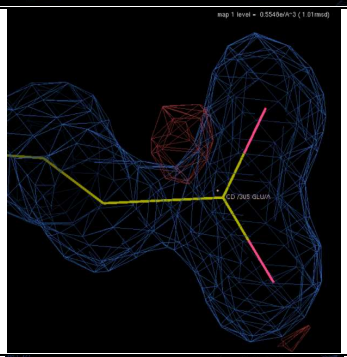	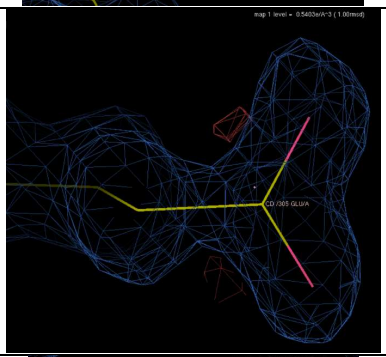	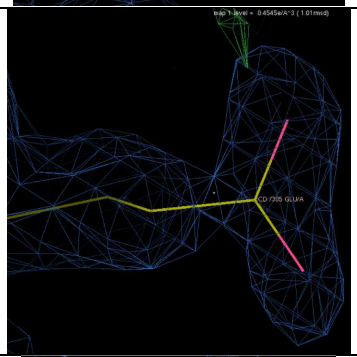
Glu315	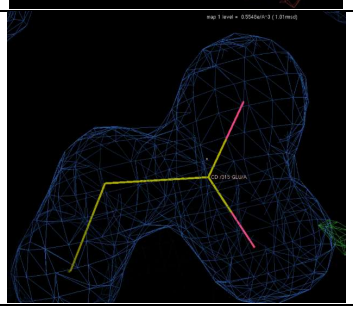	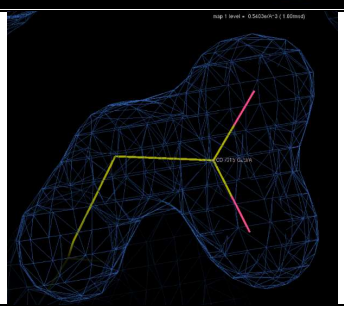	

Glu292	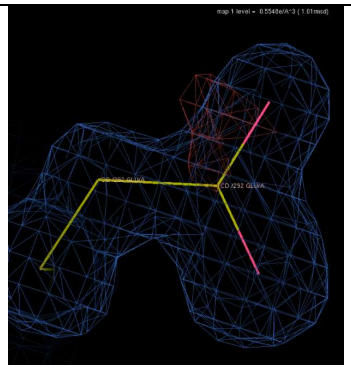	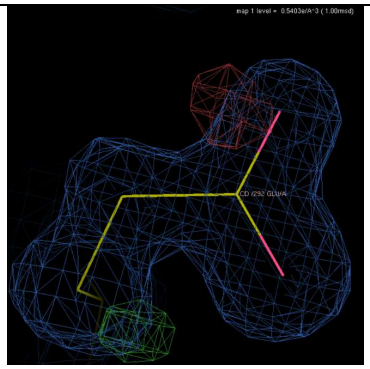	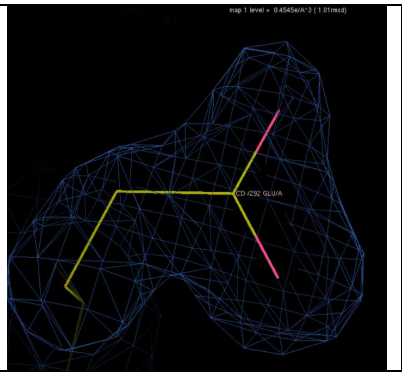

Residue	**Dataset 1 100 K**	**Dataset 2 150 K**	**Dataset 3 200 K**
Asp150	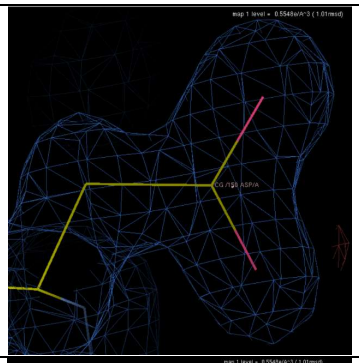	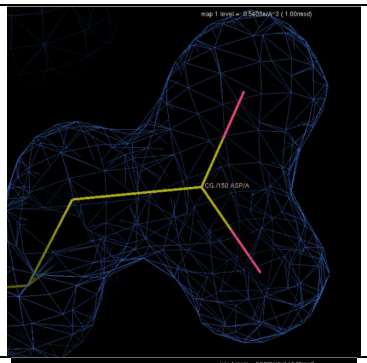	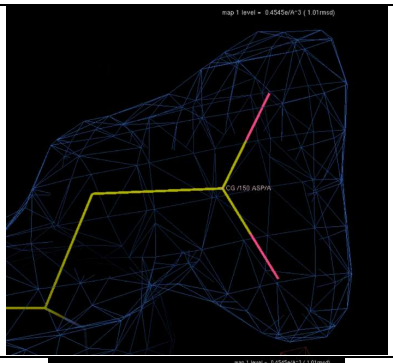
Asp385	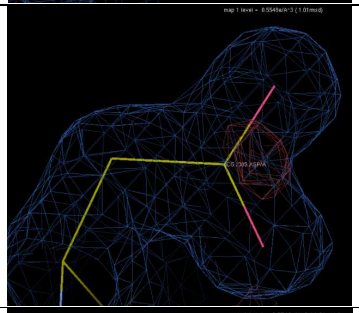	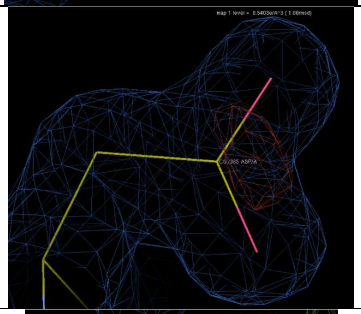	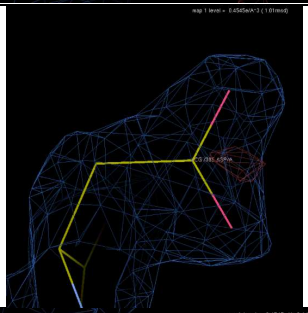
Glu172	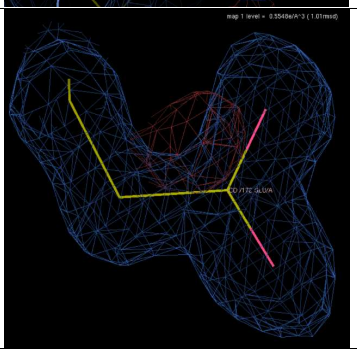	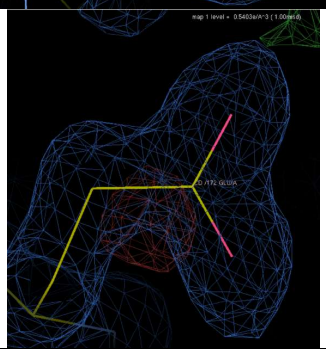	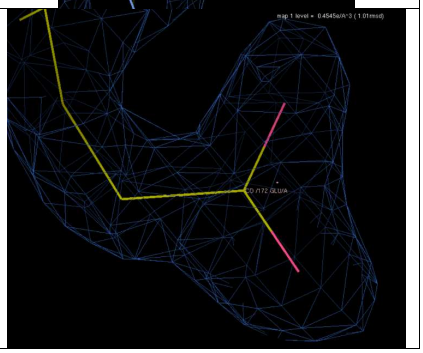

Asp335	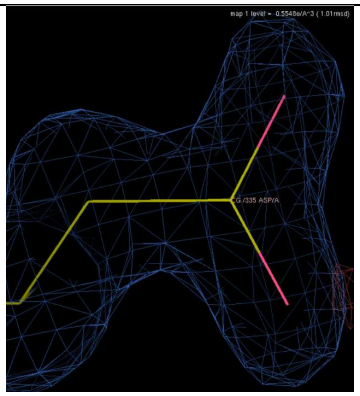	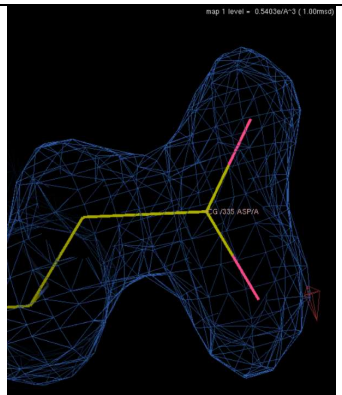	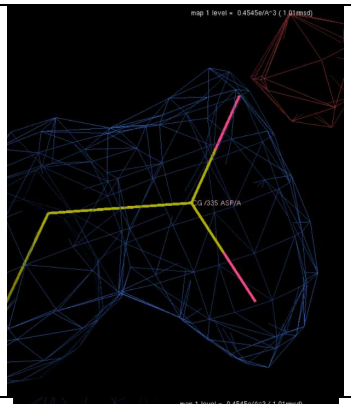
Asp340	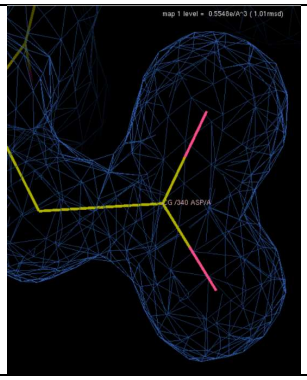	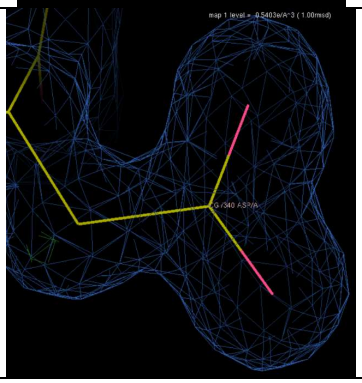	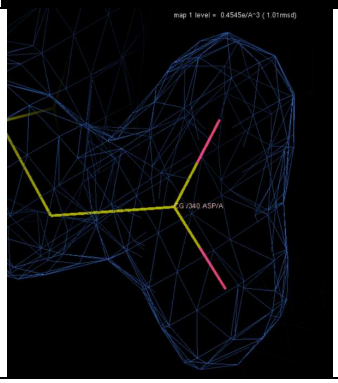

Residue	Dataset 1 100 K	Dataset 2 150 K	Dataset 3 200 K
Asp337	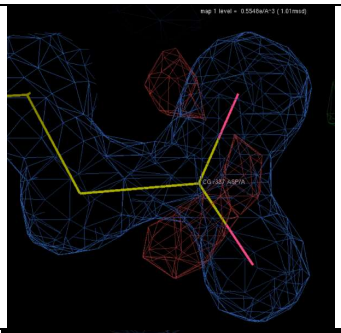	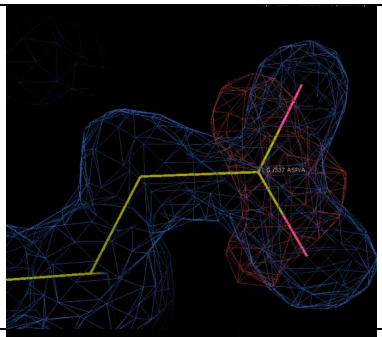	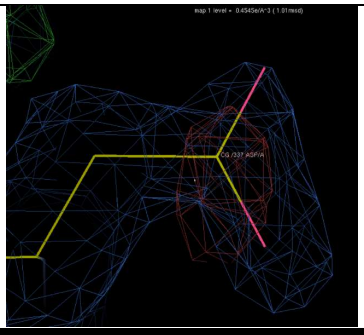
Glu88	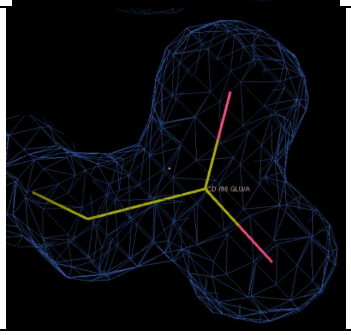	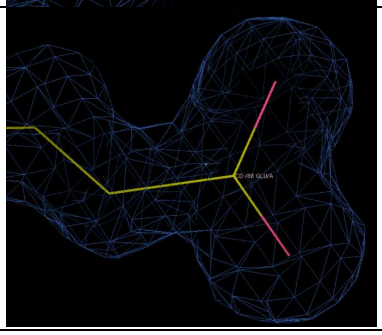	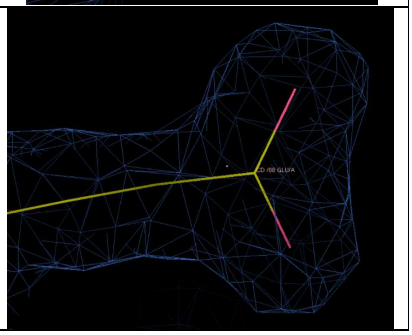

Glu286	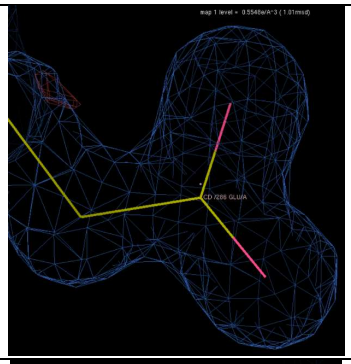	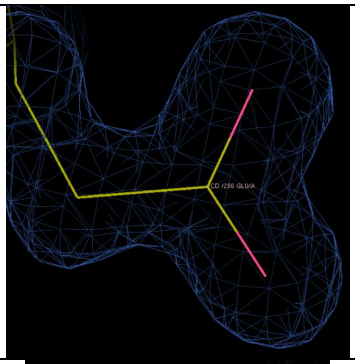	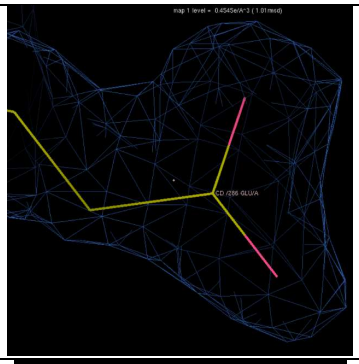
Glu369	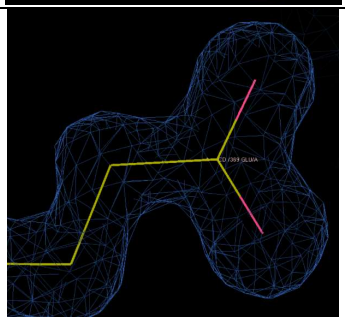	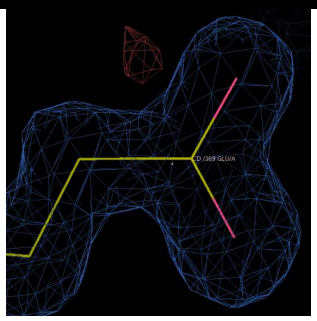	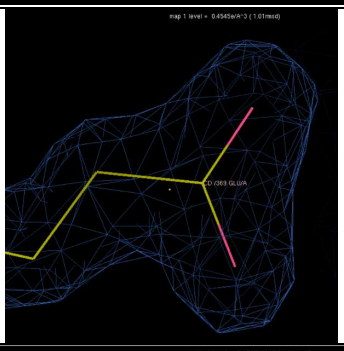
Asp137	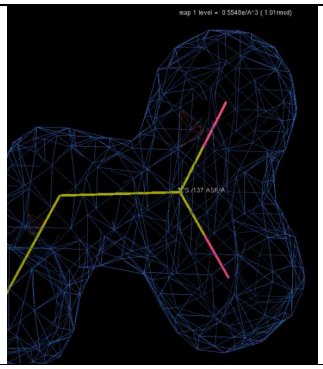	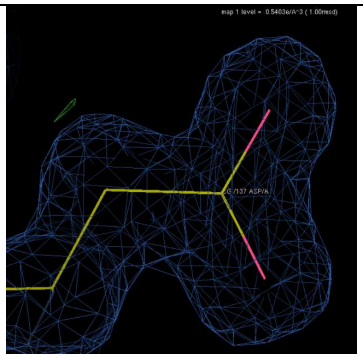	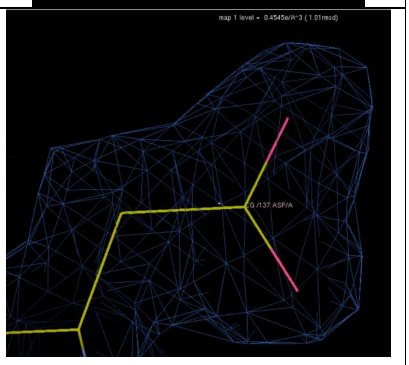

Table S7. Electron density maps of Met residues in the three successive datasets at 100, 150 and 200 K.

The $2mF_o$-DF_c electron density map is shown contoured at 1.0 σ (blue mesh), and the mF_o-DF_c difference map is shown contoured at ± 3 σ (red and green mesh).

Residue	Dataset 1 100 K	Dataset 2 150 K	Dataset 3 200 K
Met121	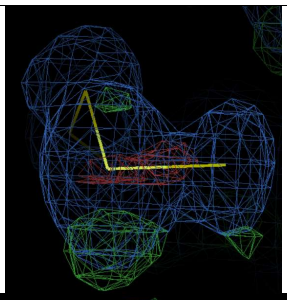	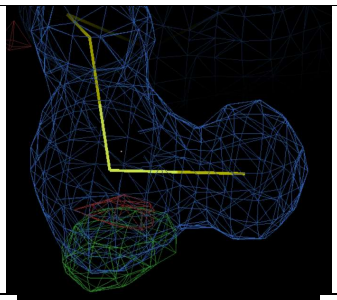	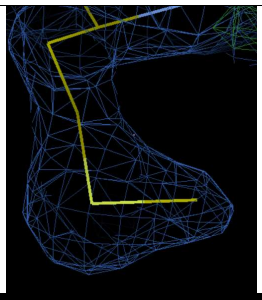
Met164	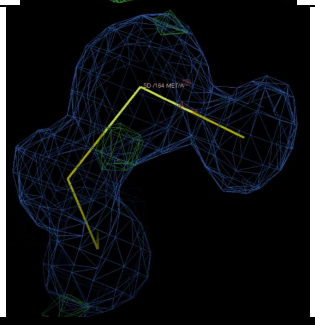	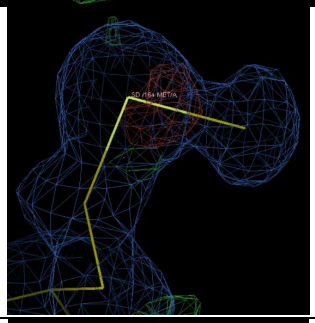	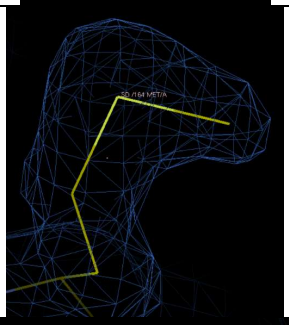
Met321	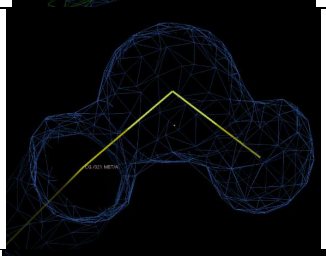		
Met371	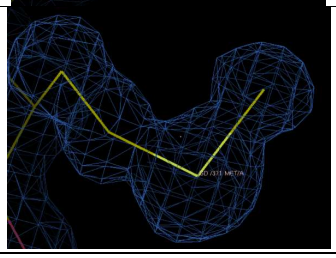	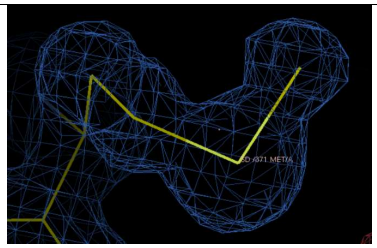	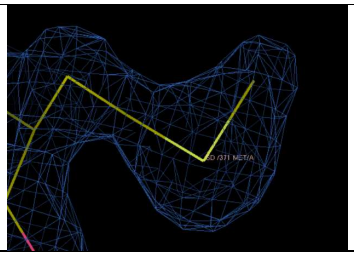

Table S8. Electron density maps of Tyr residues in the three successive datasets at 100, 150 and 200 K.

The $2mF_o$-DF_c electron density map is shown contoured at 1.0 σ (blue mesh), and the mF_o-DF_c difference map is shown contoured at ± 3 σ (red and green mesh).

Residue	Dataset 1 100 K	Dataset 2 150 K	Dataset 3 200 K
Tyr56	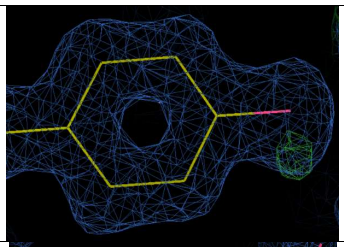	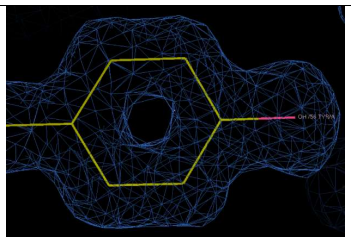	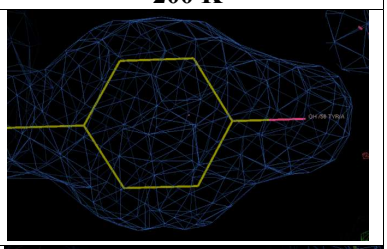
Tyr35	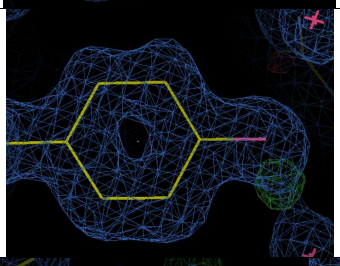	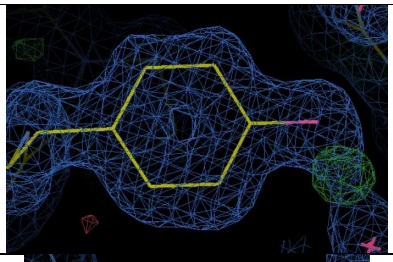	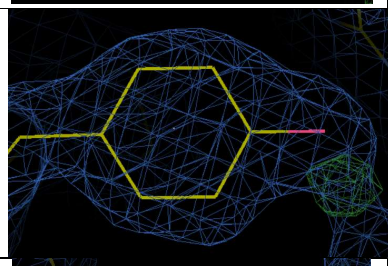
Tyr49	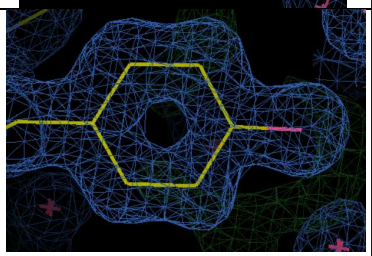	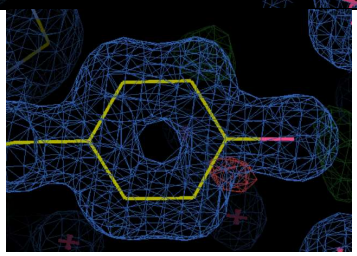	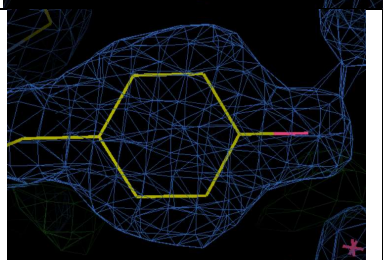
Tyr61	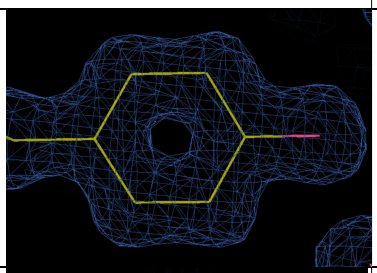	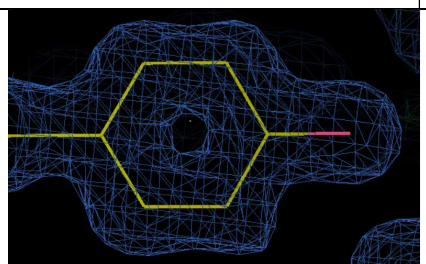	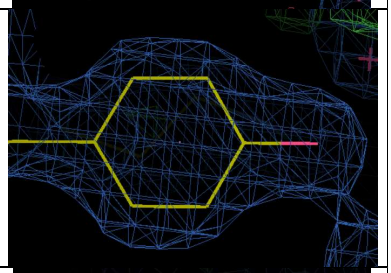
Tyr155	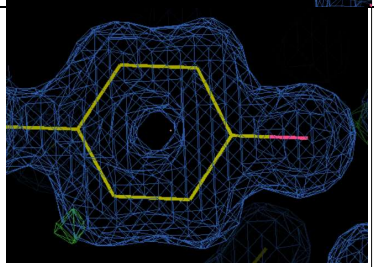	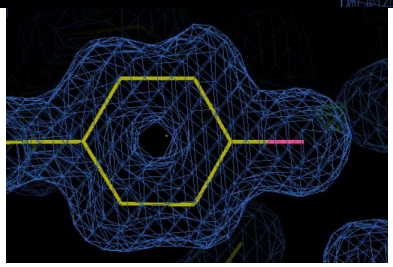	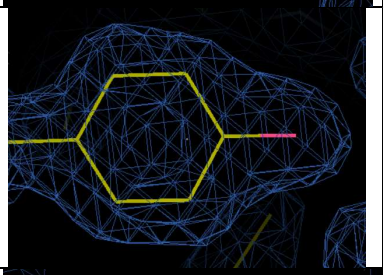
Tyr177	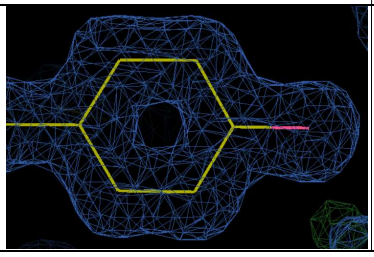	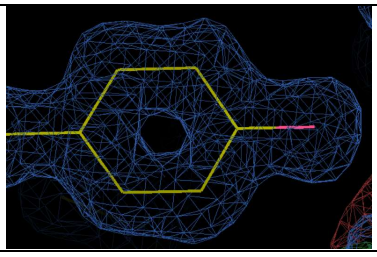	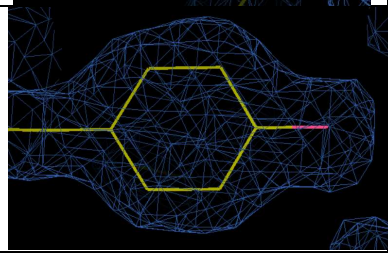

The crystal structure of 3-methylaminobenzoic acid-bound CYP199A4 (decreasing temperature experiments)

Table S9. Crystallographic data table for the crystal structures of CYP199A4 in complex with 3-methylaminobenzoic acid at 200, 150 and 100 K (decreasing temperature series). The space group is $P12_11$.

	The crystal structure of CYP199A4 bound to 3-methylaminobenzoic acid		
	Dataset 1: 200 K	**Dataset 2: 150 K**	**Dataset 3: 100 K**
PDB code	**9PLS**	**9PMA**	**9PMC**
Wavelength (Å)	0.95366	0.95366	0.95366
a/b/c (Å)	44.26/51.59/79.29	44.12/51.45/79.12	44.18/51.37/78.98
α/β/γ (˚)	90.00/92.19/90.00	90.00/92.26/90.00	90.00/92.16/90.00
Resolution (Å)	44.23-1.76 (1.80-1.76)	44.08-1.75 (1.78-1.75)	44.15-1.51 (1.53-1.51)
<I/σ(I)>	8.2 (1.0)	8.2 (0.9)	9.2 (1.0)
Unique reflections	35271	35720	55656
Completeness	99.3 (89.8)	98.5 (74.9)	99.0 (82.3)
Redundancy	6.7 (6.2)	6.6 (5.9)	6.8 (6.3)
R_{merge} (%) (all I+ and I-)	13.0 (135.2)	12.2 (143.8)	10.8 (181.4)
R_{pim} (%) (all I+ and I-)	5.4 (57.9)	5.1 (62.3)	4.4 (75.9)
$CC_{1/2}$	99.7 (61.0)	99.8 (50.8)	99.9 (59.5)
R_{work} (%)	16.80	17.14	17.03
R_{free} (%)	19.88	19.48	20.63
r.m.s.d. bond lengths (Å)	0.003	0.002	0.005
r.m.s.d. bond angles (˚)	0.663	0.531	0.763
Ramachandran plot (%)			
Most favoured	97.95	97.70	98.47
Allowed	2.05	2.3	1.53
Outliers	0	0	0
Average B-factor (Å²)	25.92	26.26	22.01

Displacement of the iron below the heme plane in the crystal structures of CYP199A4 bound to 3-methylaminobenzoic acid (decreasing temperature series)

Table S10. Displacement of the iron below the heme plane in the crystal structures of CYP199A4 bound to 3-methylaminobenzoic acid (decreasing temperature series)

Dataset	Temperature	Displacement of the iron below the heme plane*	Fe-S bond length
1	200 K	0.23 Å	2.41 Å
2	150 K	0.16 Å	2.48 Å
3	100 K	0.22 Å	2.38 Å

* plane defined by the four pyrrole nitrogens

Displacements were measured using UCSF Chimera.

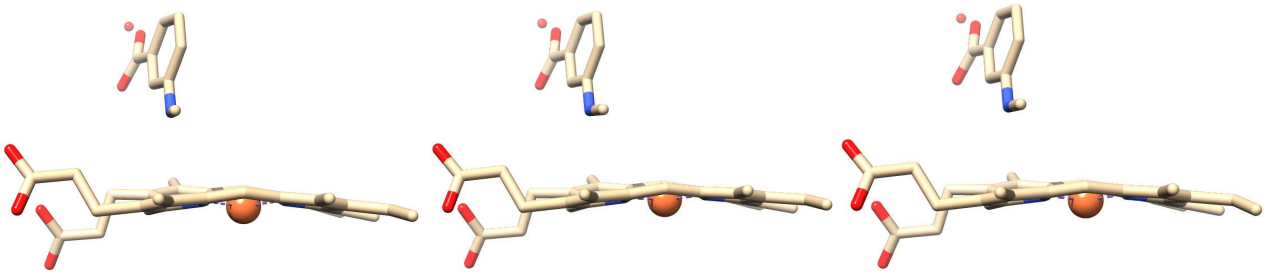

200 K **150 K** **100 K**

Figure S20. Displacement of the iron below the heme plane in the crystal structures of CYP199A4 bound to 3-methylaminobenzoic acid at 200, 150 and 100 K (decreasing temperature series).

Dataset 1: The crystal structure of CYP199A4 bound to 3-methylaminobenzoic acid solved at 200 K

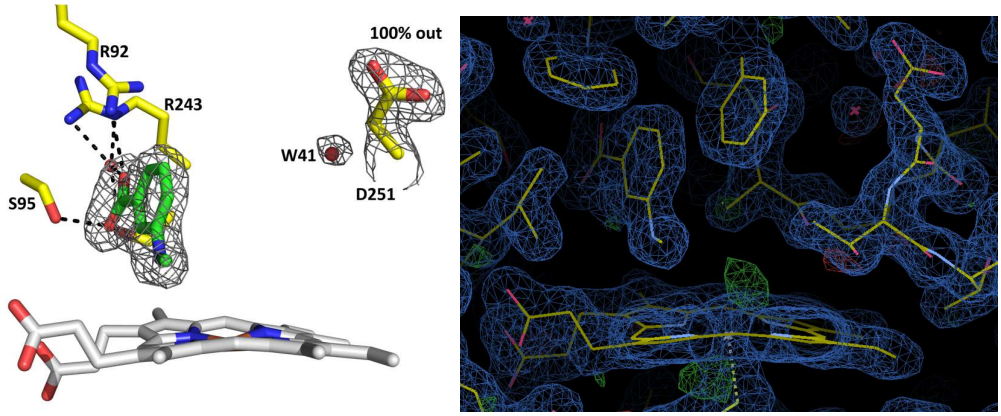

Figure S21. The crystal structure of CYP199A4 bound to 3-methylaminobenzoic acid solved at **200 K** (**1.76-Å** resolution). A *2mFo-DFc* composite omit map of the substrate, W41 and D251 side chain is shown as grey mesh contoured at 1.0 σ (1.5 Å carve). The D251 side chain points entirely out of the active site into the solvent channel. The image on the right shows the *2mFo-DFc* map contoured at 1.0 σ (blue mesh) and the *mFo-DFc* difference map contoured at ± 3.0 σ (red/green mesh).

Dataset 2: The crystal structure of CYP199A4 bound to 3-methylaminobenzoic acid solved at 150 K

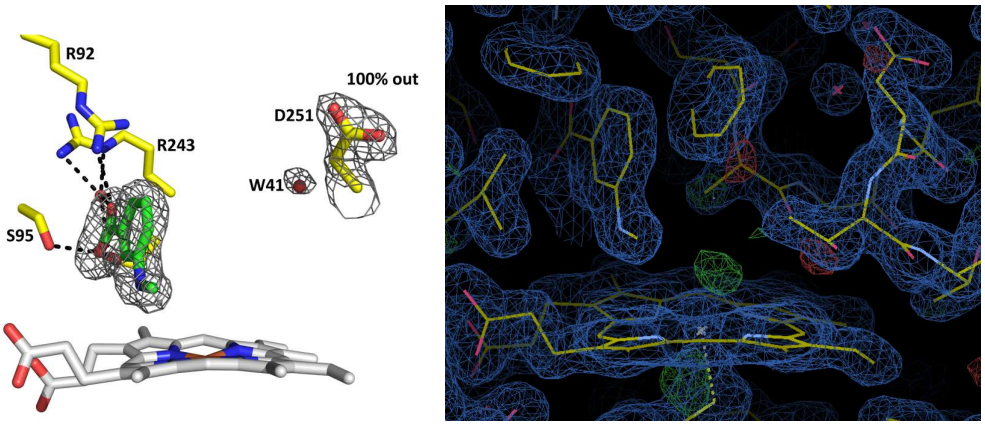

Figure S22. The crystal structure of CYP199A4 bound to 3-methylaminobenzoic acid solved at **150 K** (**1.75-Å** resolution). A *2mFo-DFc* composite omit map of the substrate, W41 and D251 side chain is shown as grey mesh contoured at 1.0 σ (1.5 Å carve). The D251 side chain points entirely out of the active site into the solvent channel. The image on the right shows the *2mFo-DFc* map contoured at 1.0 σ (blue mesh) and the *mFo-DFc* difference map contoured at ± 3.0 σ (red/green mesh).

Dataset 3: The crystal structure of CYP199A4 bound to 3-methylaminobenzoic acid solved at 100 K

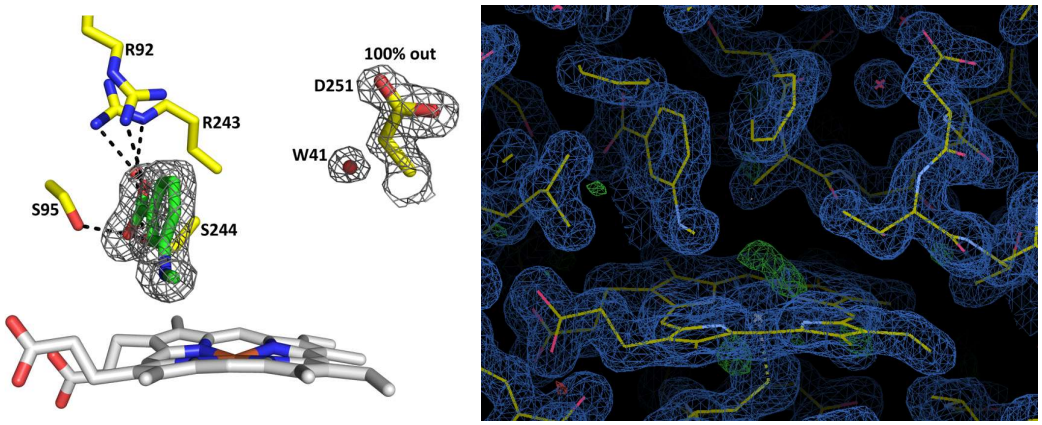

Figure S23. The crystal structure of CYP199A4 bound to 3-methylaminobenzoic acid solved at **100 K** (**1.51-Å** resolution). A *2mFo-DFc* composite omit map of the substrate, W41 and D251 side chain is shown as grey mesh contoured at 1.0 σ (1.5 Å carve). The D251 side chain points entirely out of the active site into the solvent channel. The image on the right shows the *2mFo-DFc* map contoured at 1.0 σ (blue mesh) and the *mFo-DFc* difference map contoured at ± 3.0 σ (red/green mesh).

In all three structures (Figure S21-23), the D251 side chain points fully out of the active site, the high-occupancy heme-aqua ligand is not present, the carbonyl of A248 has moved away from the heme, and the methylamino group of the substrate has rotated inwards towards the heme. In all three structures a small difference map density peak was visualized near the heme. This could correspond to a very low occupancy water. However, addition of a water molecule in the structure and subsequent refinement lead to a very low occupancy water at that position which was removed automatically and did not justify modelling.

***In crystallo* movement of D251 in a crystal of CYP199A4 bound to 4-phenoxybenzoic acid**

Table S11. Crystallographic data table for the crystal structures of CYP199A4 in complex with 4-phenoxybenzoic acid at 100, 150 and 200 K (increasing temperature series). The space group is $P12_11$.

	The crystal structure of CYP199A4 bound to 4-phenoxybenzoic acid		
	Dataset 1: 100 K	**Dataset 2: 150 K**	**Dataset 3: 200 K**
PDB code	**9ZEG**	**9ZEH**	**9ZEI**
Wavelength (Å)	0.95373	0.95373	0.95373
a/b/c (Å)	44.35/51.47/78.92	44.42/51.56/79.02	44.45/51.70/79.24
α/β/γ (°)	90.00/92.19/90.00	90.00/92.20/90.00	90.00/92.26/90.00
Resolution (Å)	44.32-1.53 (1.56-1.53)	44.39-1.51 (1.54-1.51)	44.42-1.74 (1.77-1.74)
<I/σ(I)>	9.2 (1.1)	9.4 (0.9)	9.3 (1.0)
Unique reflections	53240	55691	37236
Completeness	98.8 (87.2)	99.1 (86.2)	99.5 (96.3)
Redundancy	6.7 (6.7)	6.8 (6.6)	6.8 (6.6)
R_{merge} (%) (all I+ and I-)	14.1 (201.5)	11.3 (185.4)	10.7 (139.8)
R_{pim} (%) (all I+ and I-)	5.9 (82.8)	4.7 (77.0)	4.4 (58.2)
$CC_{1/2}$	99.7 (53.0)	99.8 (52.6)	99.8 (60.8)
R_{work} (%)	17.10	15.95	15.85
R_{free} (%)	19.99	18.45	19.72
r.m.s.d. bond lengths (Å)	0.006	0.012	0.004
r.m.s.d. bond angles (°)	0.856	1.183	0.736
Ramachandran plot (%)			
Most favoured	97.70	98.21	98.21
Allowed	2.30	1.53	1.79
Outliers	0	0.26	0
Average B-factor (Å^2)	21.53	22.34	27.10

Table S12. Position of the D251 side chain in the variable-temperature structures of CYP199A4 bound to 4-phenoxybenzoic acid

Dataset	**Temperature**	**Occupancy of D251 conformation pointing into active site**	**Occupancy of D251 conformation pointing out of the active site (into the solvent channel)**
1	**100 K**	27%	73%
2	**150 K**	Not present	100%
3	**200 K**	Not present	100%

Table S13. Occupancy of the heme-bound aqua ligand in the variable-temperature structures of CYP199A4 bound to 4-phenoxybenzoic acid

Dataset	**Temperature**	**Refined occupancy of the heme-bound aqua ligand**
1	**100 K**	70%
2	**150 K**	44%
3	**200 K**	59%

Comparison of the new and previously determined crystal structures of CYP199A4 bound to 4-phenoxybenzoic acid at 100 K

The structure of 4-phenoxybenzoic acid-bound CYP199A4 was previously determined at 100 K (PDB code: 7TND). The resolution of this previously reported structure is 1.82 Å.

The new 100 K structure was determined at higher resolution (1.53-Å resolution) and is broadly consistent with the previously determined structure. In both structures, a high-occupancy heme-bound aqua ligand is present (~70% occupancy). In the previously determined structure, a second conformation of the D251 side chain was not observed. In the new structure, the D251 side chain has electron density consistent with the D251 side chain being located both in and out of the active site (27% occupancy, Table S?)).

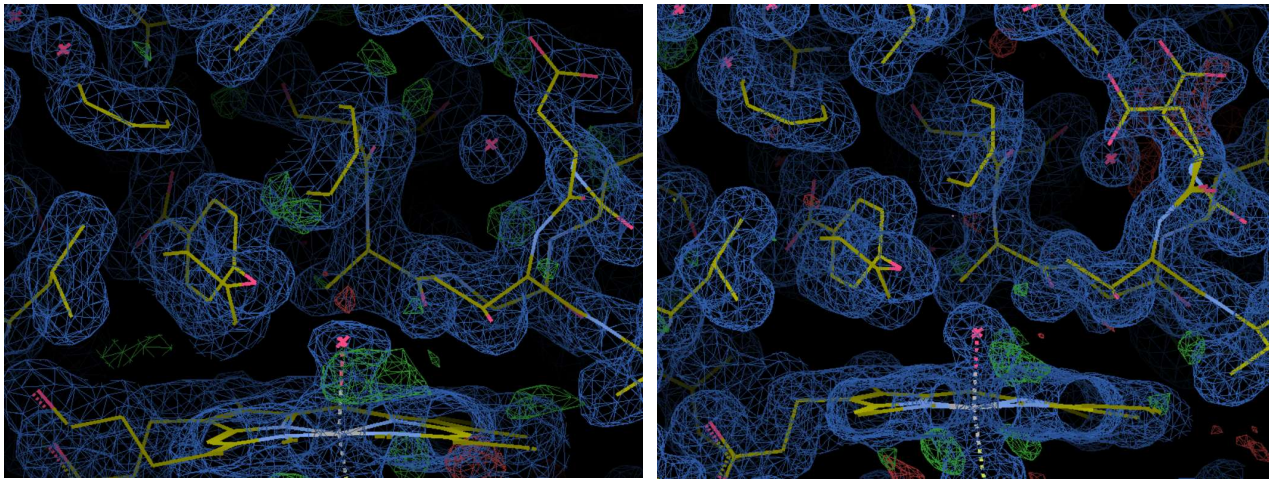

Previously solved structure (PDB code: 7TND; 1.82 Å resolution) **New structure (1.53-Å resolution)**

Figure S24. Comparison the new and previously determined crystal structures of CYP199A4 bound to 4-phenoxybenzoic acid at 100 K. The $2mF_o$-DF_c electron density map is shown as blue mesh contoured at 1.0 or 0.7 σ, and the mF_o-DF_c difference map is shown as green and red mesh contoured at ± 3.0 σ.

Table S14. Table of occupancy data for the crystal structures of CYP199A4 bound to 4-phenoxybenzoic acid determined at 100 K

	Occupancy (%)	
	Previously solved structure (7TND)	**New 100 K structure**
Heme-bound aqua ligand	74%	70%
Substrate	100%	100%
D251 conformation pointing into active site	Not present	27%
D251 conformation pointing out of active site (into water channel)	100%	73%

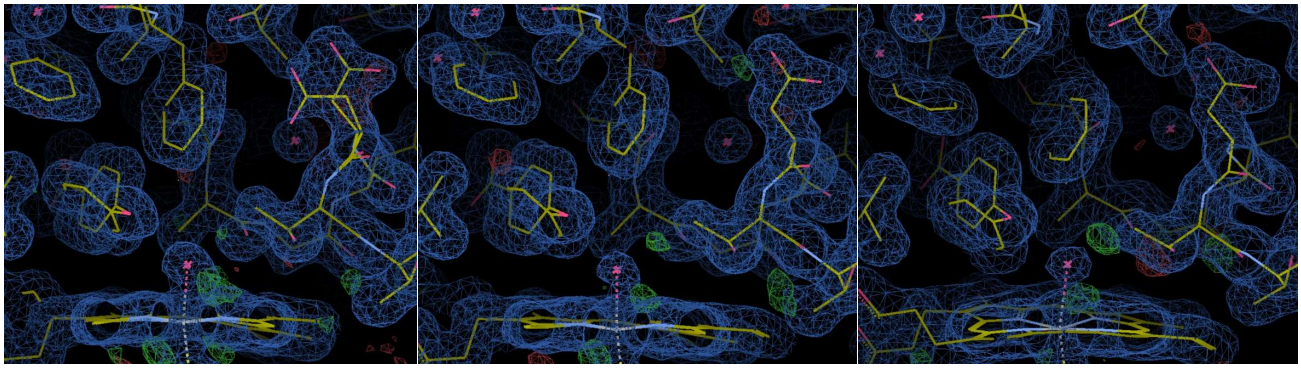

100 K **150 K** **200 K**

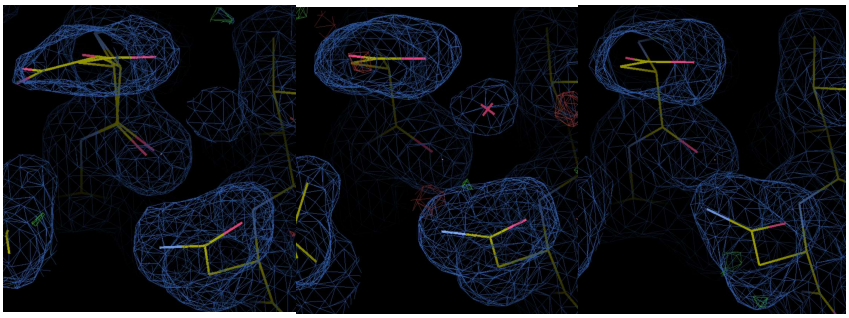

100 K **150 K** **200 K**

Figure S25. Above: The crystal structures of 4-phenoxybenzoic acid-bound WT CYP199A4 at 100, 150 and 200 K. The $2mF_o$-DF_c maps are shown as blue mesh contoured at 0.7 σ. **Below:** As the temperature is raised, the D251 conformation pointing into the active site disappears, and the N255 side chain also rotates towards D251.

Table S15. Displacement of the iron below the heme plane in the crystal structures of CYP199A4 bound to 4-phenoxybenzoic acid.

Dataset	Temperature	Displacement of the iron below the heme plane*	Fe-S bond length
1	100 K	0.140	2.30 Å
2	150 K	0.190	2.36 Å
3	200 K	0.192	2.37 Å

* plane defined by the four pyrrole nitrogens

Displacements were measured using UCSF Chimera.

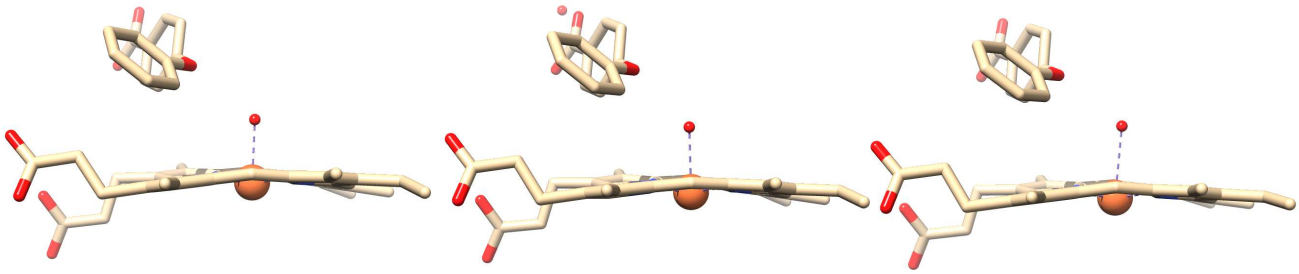

100 K **150 K** **200 K**

Figure S26. Displacement of the iron below the heme plane in the crystal structures of CYP199A4 bound to 4-phenoxybenzoic acid.

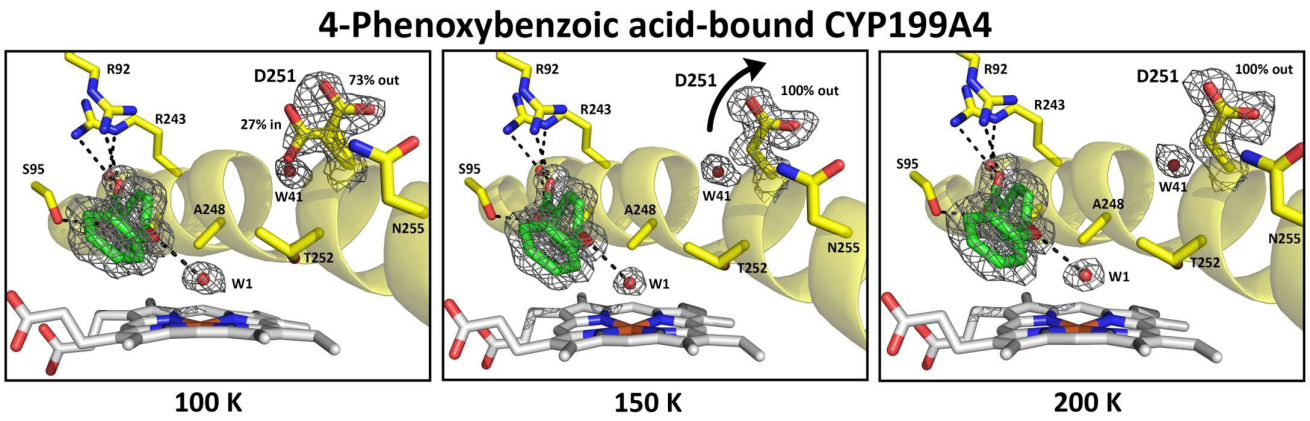

Figure S27. The crystal structures of 4-phenoxybenzoic acid-bound CYP199A4 determined at temperatures 100 K, 150 K and 200 K. A $2mF_o$-DF_c feature-enhanced map of the 4-phenoxybenzoic acid ligand, heme-aqua ligand (Wat1), W41 and D251 side chain is shown contoured at 1.0 σ.

The crystal structure of 4-phenoxybenzoic acid-bound CYP199A4 was determined at temperatures of 100, 150 and 200 K. At 200 K, the heme-bound aqua ligand has been partly retained (59% occupancy). The D251 side chain points entirely out of the active site.

Movement of A248 in the crystal structures of CYP199A4 bound to 4-phenoxybenzoic acid at 100, 150 and 200 K

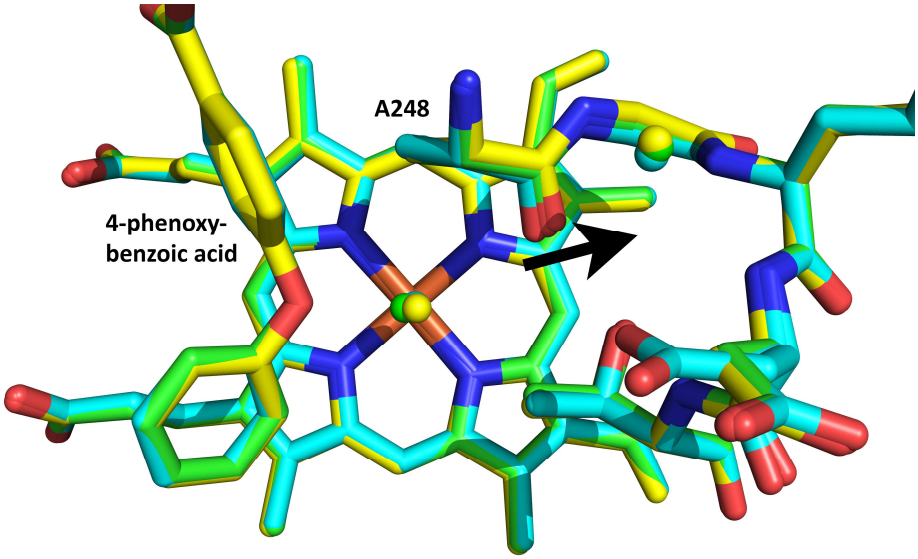

Figure S28. The overlaid crystal structures of CYP199A4 bound to 4-phenoxybenzoic acid at 100 K (cyan), 150 K (green) and 200 K (yellow). As the temperature is raised and the occupancy of the heme-bound aqua ligand decreases, the carbonyl of A248 shifts further away from the centre of the heme (movement described by the **black arrow**). The substrate does not move.

The carbonyl oxygen of A248 shifts by 0.4 Å. The hydroxyl O of T252 barely shifts (0.1 Å).

Table S16. Table of crystallographic data for the structures of CYP199A4 bound to 4-methoxybenzoic acid obtained at 100, 150, 200 and 300 K

Dataset	**1**	**2**	**3**	**4**
Temperature	**100 K**	**150 K**	**200 K**	**300 K**
PDB code	9DOE	9MJF	9MJJ	9MJK
X-ray wavelength (Å)	0.95372	0.95372	0.95372	0.95372
Unit cell (a/b/c)	44.47 51.39 79.05	44.47 51.46 79.11	44.54 51.62 79.37	44.94 52.01 79.81
(α/β/γ)	90.00 92.34 90.00	90.00 92.43 90.00	90.00 92.33 90.00	90.00 92.23 90.00
Space group	P 1 2_1 1	P 1 2_1 1	P 1 2_1 1	P 1 2_1 1
Molecules per asymmetric unit	1	1	1	1
Resolution range	44.43 - 1.26 (1.29 - 1.26)	43.12 - 1.50 (1.53 - 1.50)	44.50 - 1.39 (1.41 - 1.39)	44.91 - 2.49 (2.59 - 2.49)
<I/σ(I)>	8.9 (1.2)	13.4 (4.4)	8.0 (0.8)	1.5 (0.6)
Unique reflections	94087 (3840)	56535 (2793)	71942 (2431)	12959 (1307)
Completeness	98.7 (81.2)	98.5 (99.2)	98.3 (67.7)	98.7 (89.7)
Redundancy	6.7 (6.2)	6.4 (6.5)	6.7 (5.9)	6.1 (6.2)
R_{merge}[a] (%)	9.9 (104.6)	12.6 (76.2)	11.0 (139.2)	113.2 (379.8)
R_{pim}[a] (%)	4.2 (44.7)	5.8 (33.5)	4.6 (60.2)	49.1 (161.0)
$CC_{1/2}$	99.8 (70.0)	96.8 (60.8)	99.7 (50.6)	78.4 (29.6)
R_{work}	15.91	17.81	16.31	19.50
R_{free}[b]	17.72	19.94	17.83	25.03
Unusual rotamers (%)	0	0	0	0
r.m.s.d. bond angles (°)	0.862	0.800	0.804	0.622
r.m.s.d. bond lengths (Å)	0.004	0.003	0.004	0.003
Ramachandran plot				
Most favoured	98.72	98.21	98.47	96.93
Allowed	1.28	1.79	1.53	3.07
Outliers	0	0	0	0
Average B-factor (Å²)	15.01	14.15	19.10	18.81

Values in parentheses correspond to the highest resolution shell. [a] All I+ and I-. [b] 5% of total reflections.

Table S17. Displacement of the iron below the plane of the heme

The iron is displaced below the heme plane by 0.3 Å in all three structures. Schlichting *et al*. reported that the iron is also displaced by 0.3 Å out of the porphyrin plane in the crystal structure of ferric camphor-bound P450cam.[12]

Dataset	**Temperature**	**Displacement of the iron below the heme plane***	**Fe-S bond length**
1	100 K	0.286 Å	2.36 Å
2	150 K	0.292 Å	2.35 Å
3	200 K	0.288 Å	2.38 Å

* plane defined by the four pyrrole nitrogens

Displacements were measured using UCSF Chimera.

Dataset 1: CYP199A4 + 4-methoxybenzoic acid (T = 100 K; resolution: 1.26 Å)

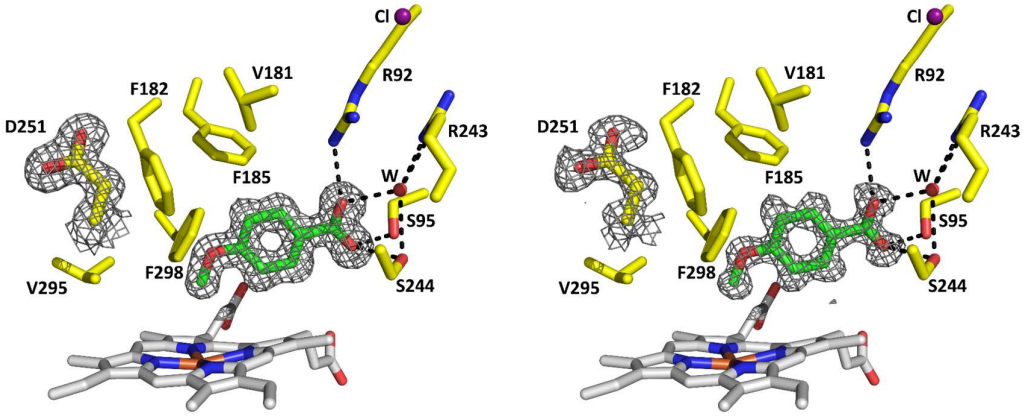

(a) Composite omit map (1.0 σ) **(b) Feature-enhanced map (1.0 σ)**

Figure S29. The crystal structure of CYP199A4 in complex with 4-methoxybenzoic acid at 100 K. A $2mF_o$-DF_c composite omit map and feature-enhanced map of the substrate and D251 side chain are shown as grey mesh contoured at 1.0 σ.

Dataset 2: CYP199A4 + 4-methoxybenzoic acid (T = 150 K; resolution: 1.50 Å)

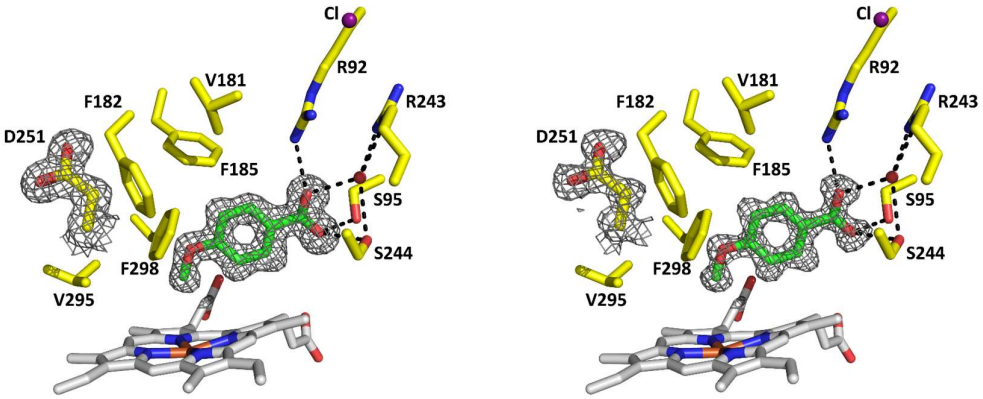

(a) Composite omit map (1.0 σ) **(b) Feature-enhanced map (1.0 σ)**

Figure S30. The crystal structure of CYP199A4 in complex with 4-methoxybenzoic acid at 150 K. A $2mF_o$-DF_c composite omit map and feature-enhanced map are shown as grey mesh contoured at 1.0 σ.

Dataset 3: CYP199A4 + 4-methoxybenzoic acid (T = 200 K; resolution: 1.39 Å)

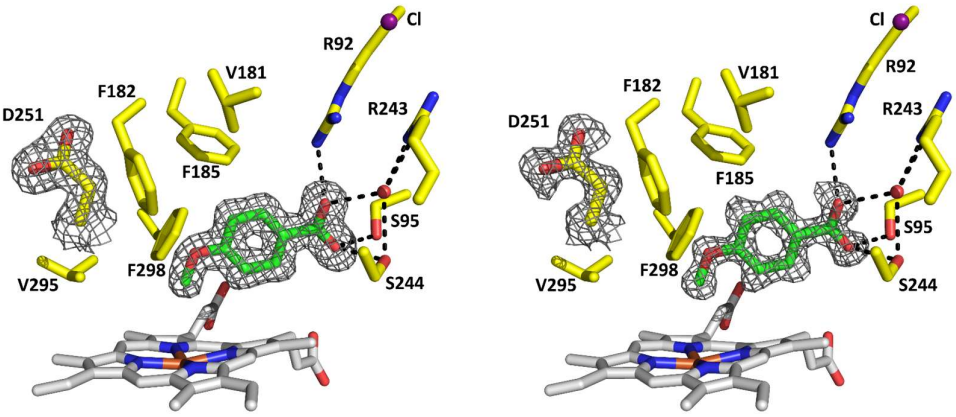

(a) Composite omit map (1.0 σ) **(b) Feature-enhanced map (1.0 σ)**

Figure S31. The crystal structure of CYP199A4 in complex with 4-methoxybenzoic acid at 200 K. A $2mF_o$-DF_c composite omit map and feature-enhanced map are shown as grey mesh contoured at 1.0 σ.

Dataset 4: CYP199A4 + 4-methoxybenzoic acid (T = 300 K; resolution: 2.49 Å)

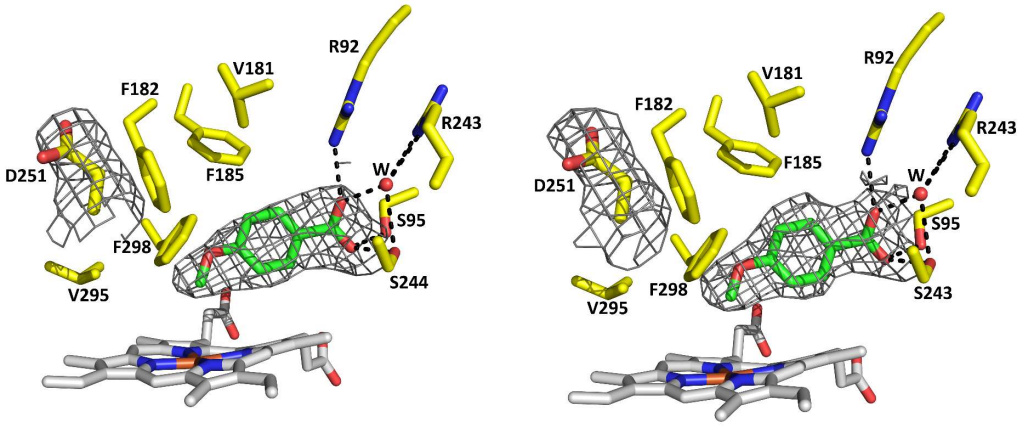

(a) Composite omit map (1.0 σ) **(b) Feature-enhanced map (1.0 σ)**

Figure S32. The crystal structure of CYP199A4 in complex with 4-methoxybenzoic acid at a temperature of 300 K (each dataset was collected using the same crystal). No movement of the acidic D251 residue was detected as the temperature was raised. A $2mF_o$-DF_c composite omit map and feature-enhanced map are shown as grey mesh contoured at 1.0 σ.

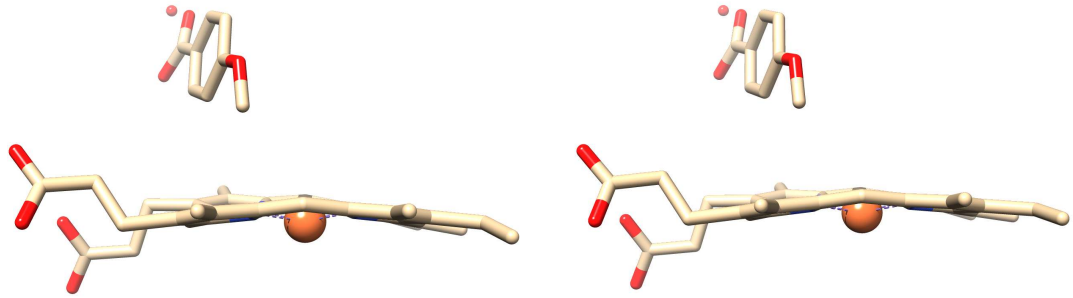

100 K **200 K**

Figure S33. Figures showing the position of the heme iron in the crystal structures of CYP199A4 bound to 4-methoxybenzoic acid at 100 K and 200 K. In each structure, the iron is displaced by ~0.3 Å below the heme plane.

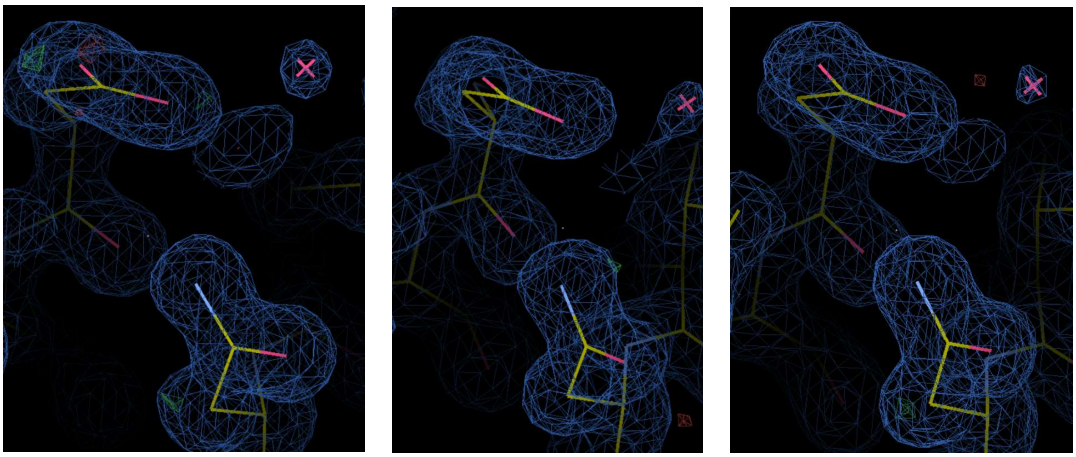

(a) 100 K **(b) 150 K** **(c) 200 K**

Figure S34. At each temperature, there is a single conformation of D251 and a single conformation of N255.

Visual inspection of the Asp/Glu residues in the 100, 200 K and 300 K crystal structures of 4-methoxybenzoic acid-bound CYP199A4 for radiation damage

Table S18. Electron density maps of Asp/Glu, Met and Tyr residues in the crystal structures of 4-methoxybenzoic acid-bound CYP199A4 at 100, 200 and 300 K. The $2mF_o$-DF_c electron density map is shown contoured at 1.0 σ (blue mesh), and the mF_o-DF_c difference map is shown contoured at ± 3.0 (red and green mesh).

Residue	Dataset 1 100 K	Dataset 3 200 K	Dataset 4 300 K
Glu367	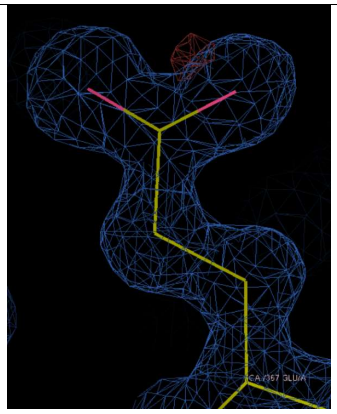		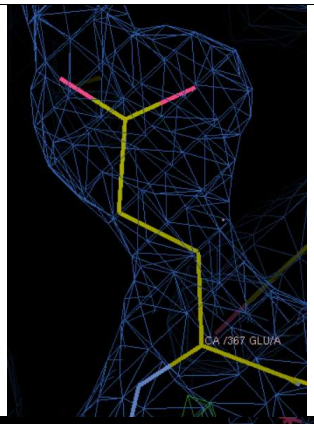
Asp33	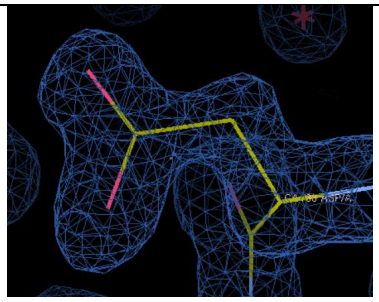	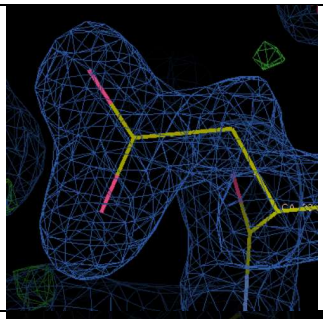	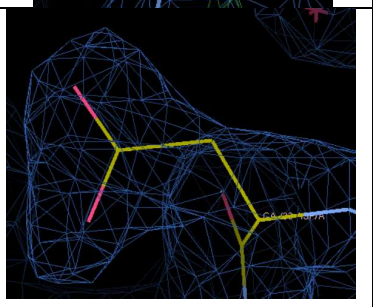
Asp277	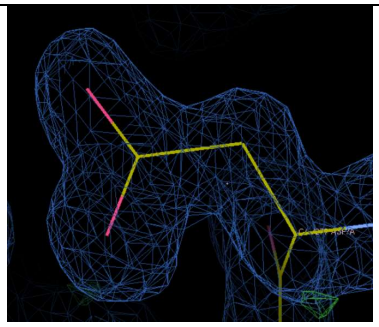	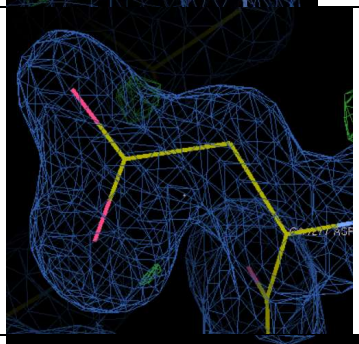	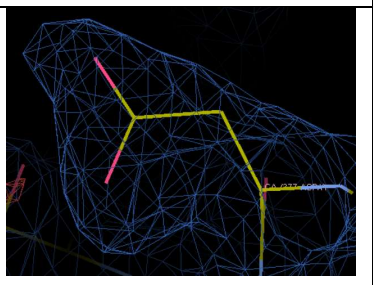
Asp236	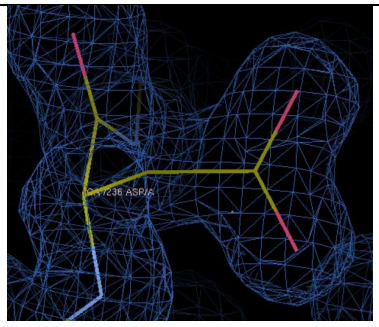	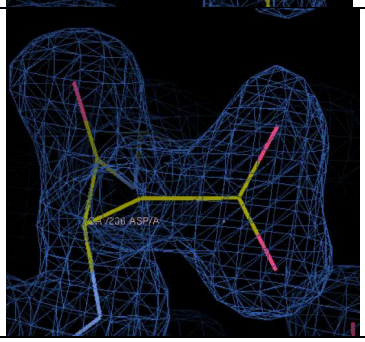	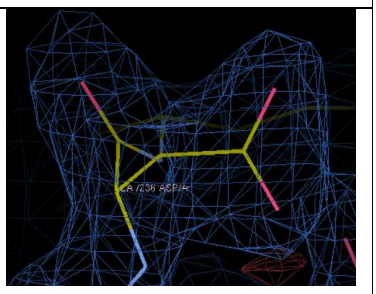

Asp70	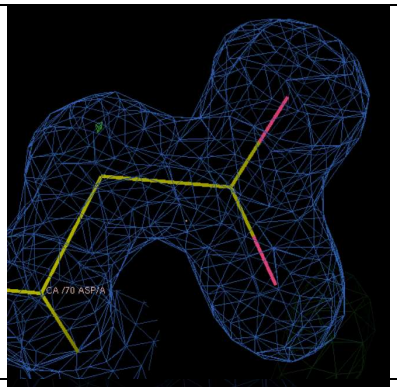	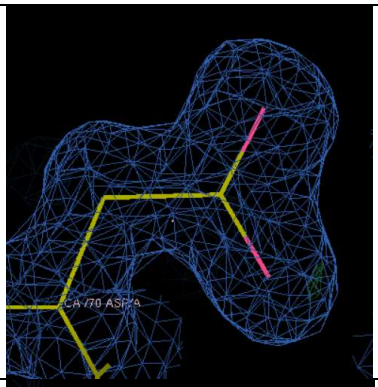	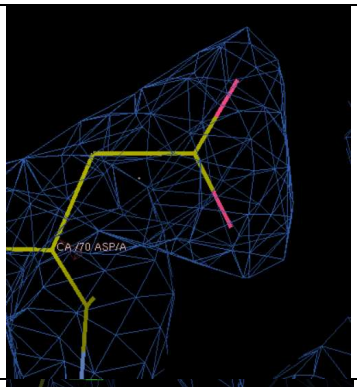
Glu63	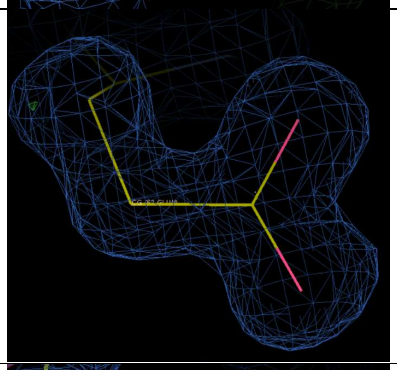	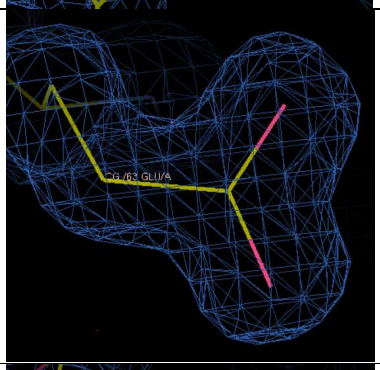	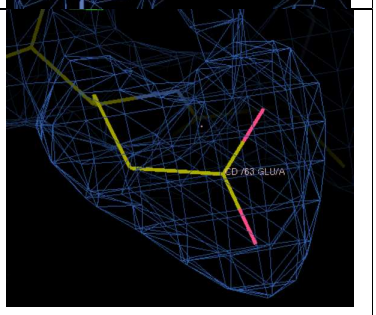
Asp329	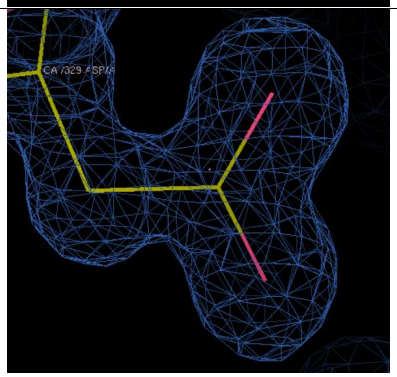	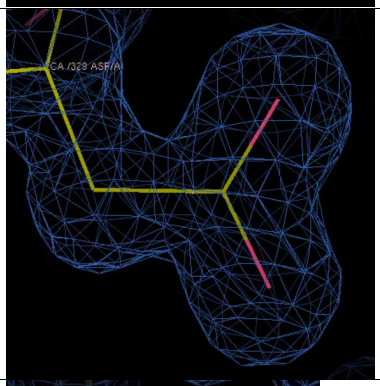	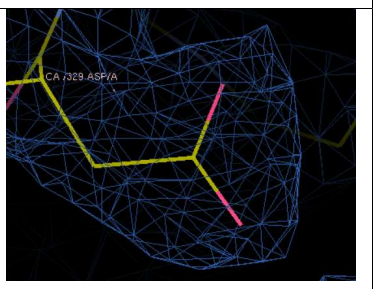
Asp251	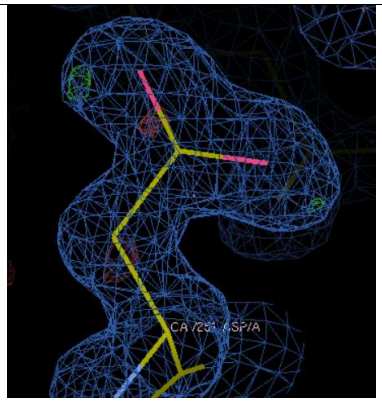	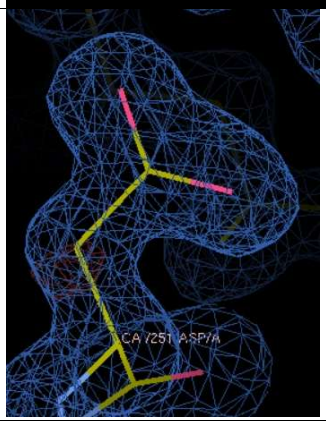	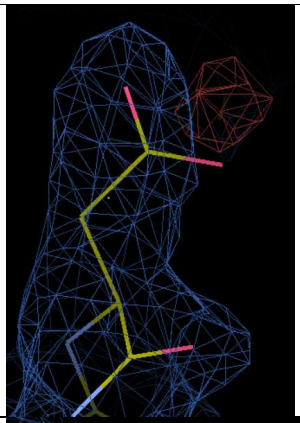
Glu305	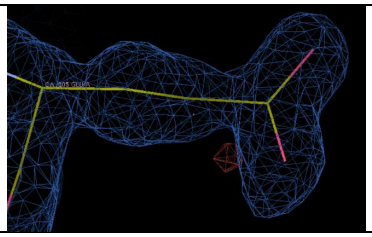	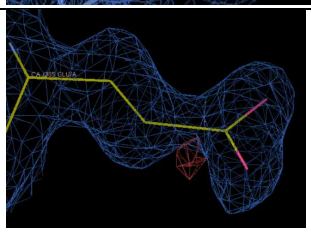	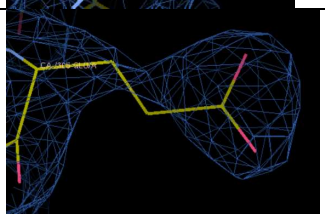

Glu315	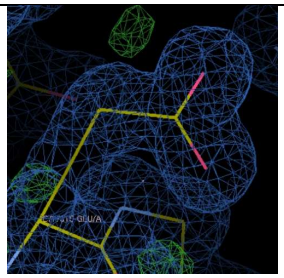	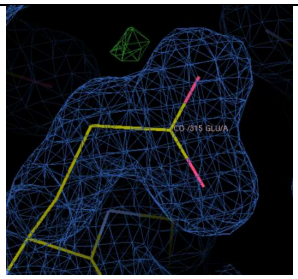	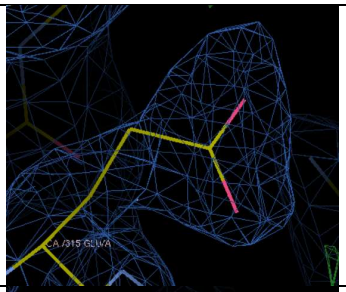
Glu292	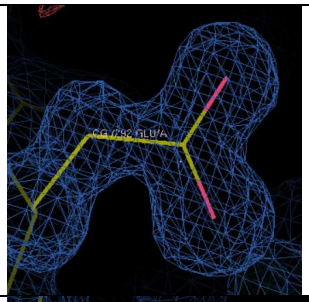	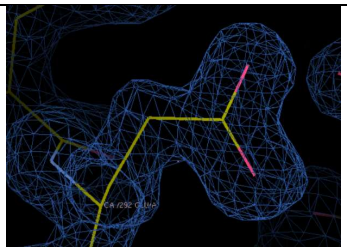	
Asp150	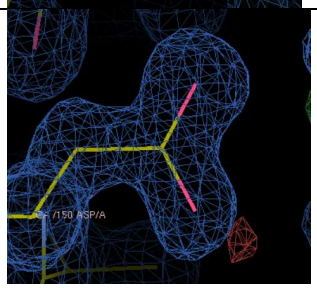	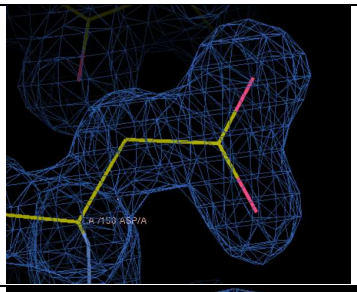	
Asp385	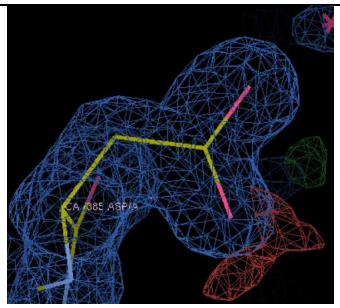	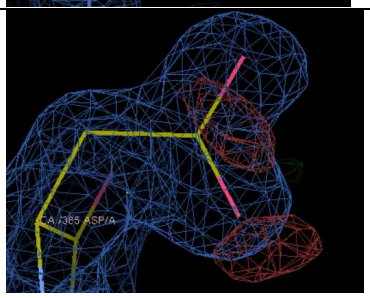	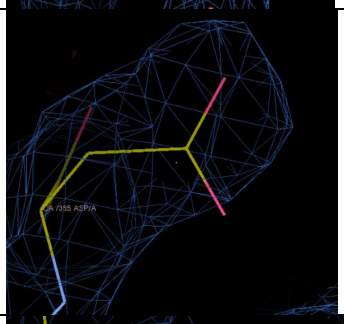
Glu172	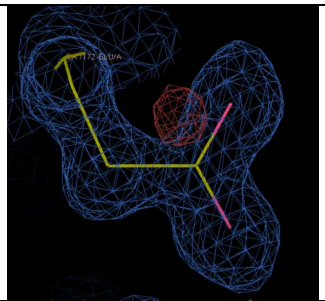	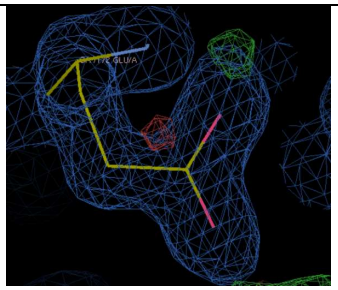	
Asp335	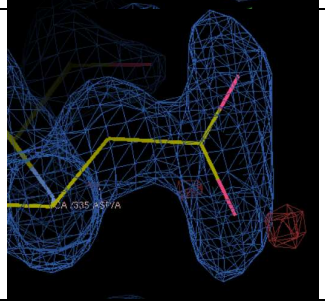	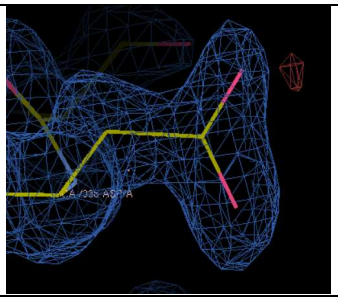	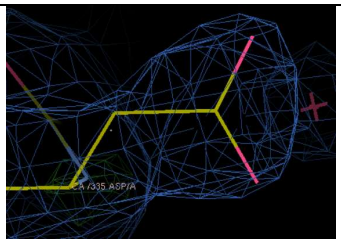

Asp340	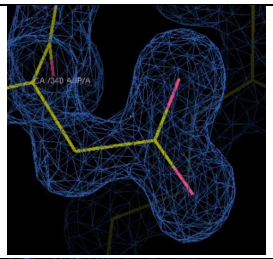	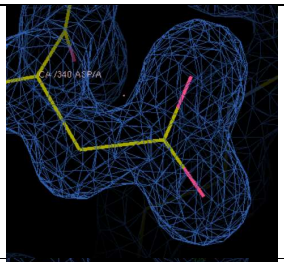	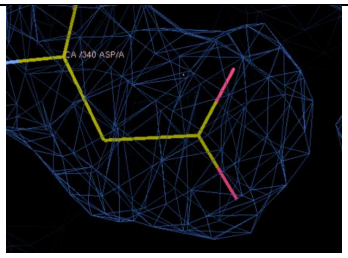
Asp337	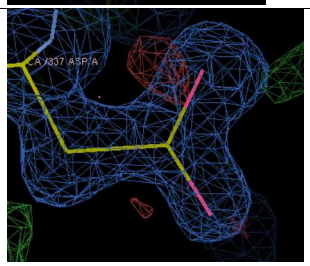	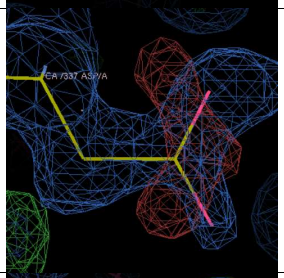	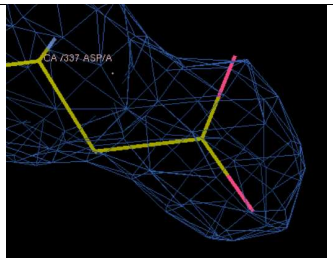
Glu88	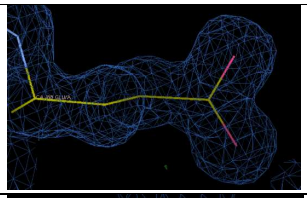	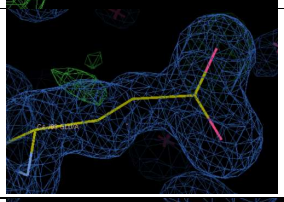	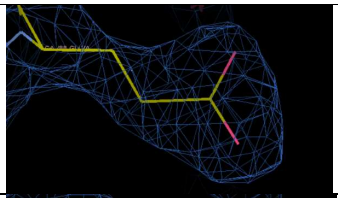
Glu286	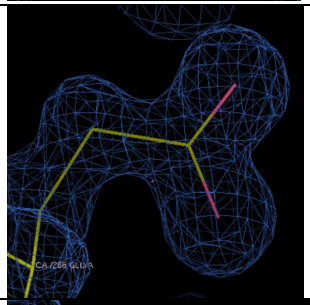		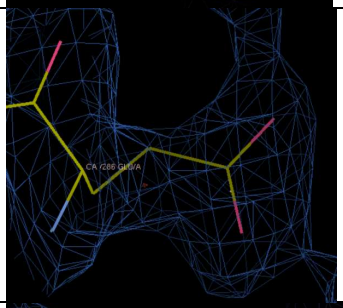
Glu369	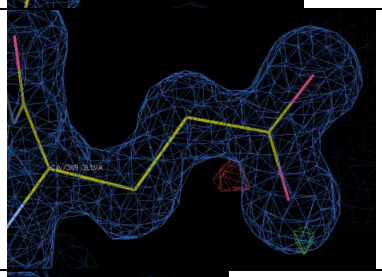		
Asp137	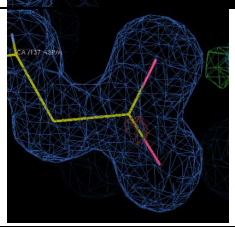		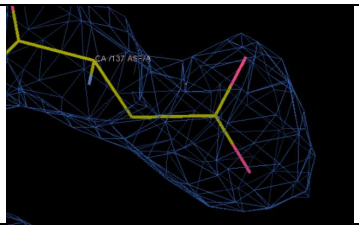
Asp126	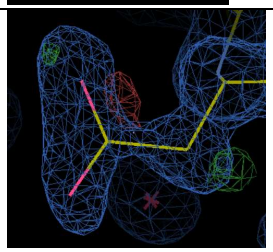	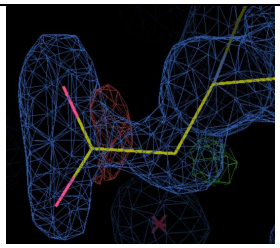	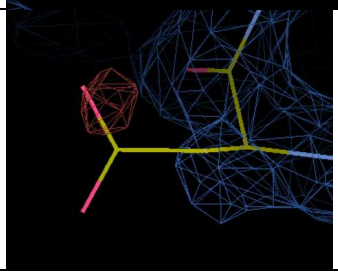

Glu400	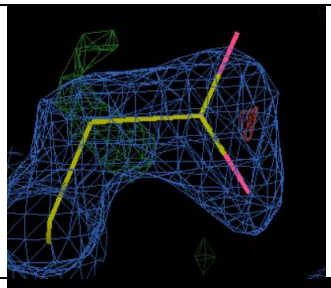	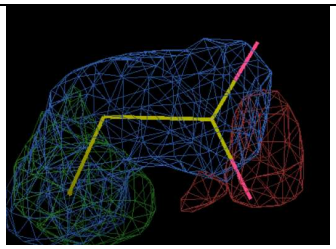	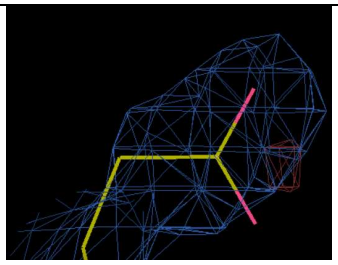
Met164	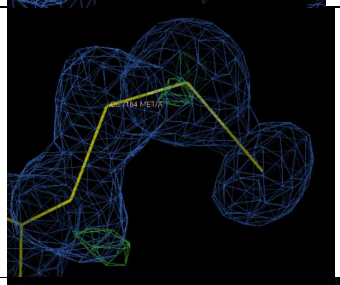	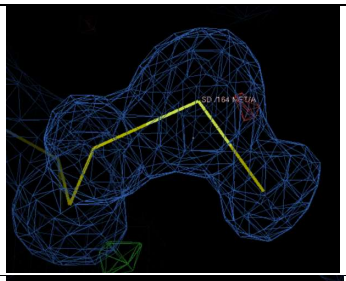	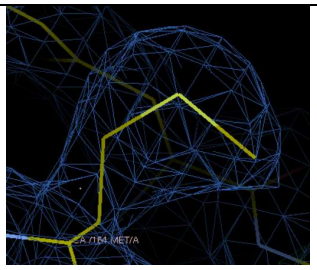
Met321	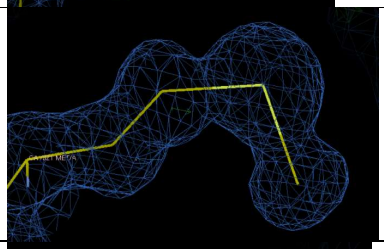	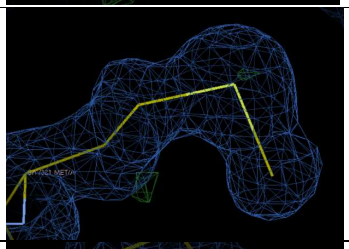	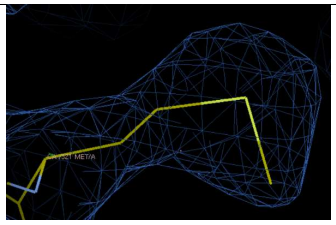
Met371	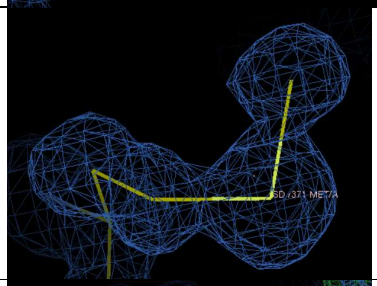	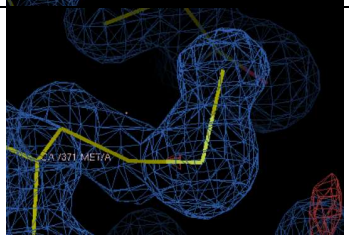	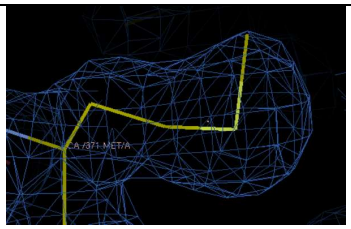
Tyr56	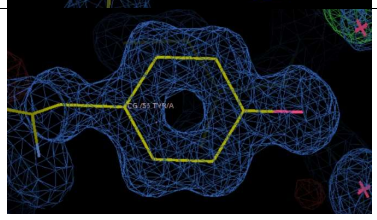	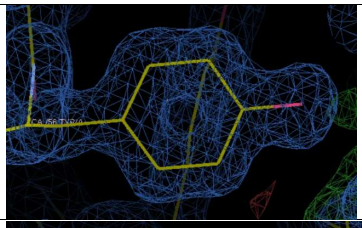	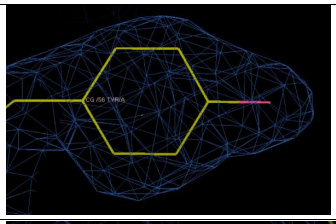
Tyr35	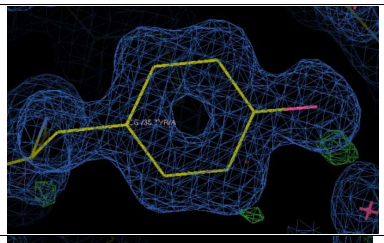	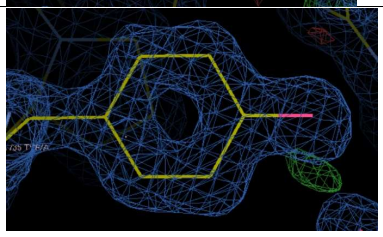	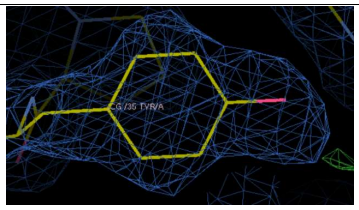
Tyr49	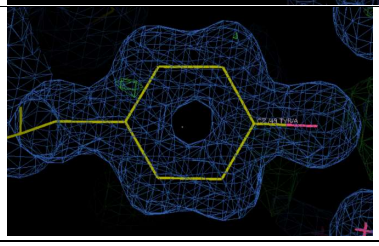	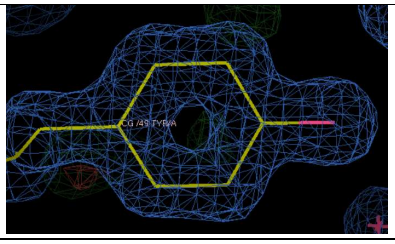	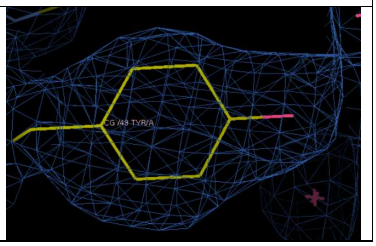

Tyr61	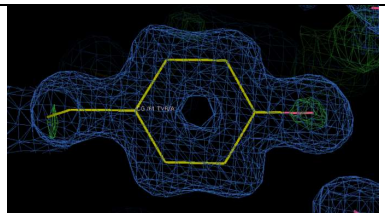	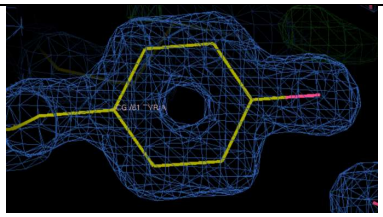	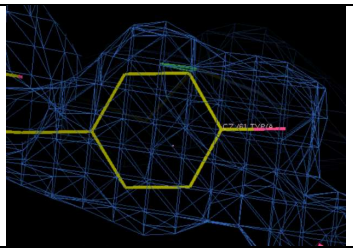

In the 300 K structure, the electron density is poorer for the D251 side chain (electron density is missing around one of the carboxylate oxygen atoms, and negative density (red mesh) appeared).

There is no electron density missing for the F182 side chain at 300 K.

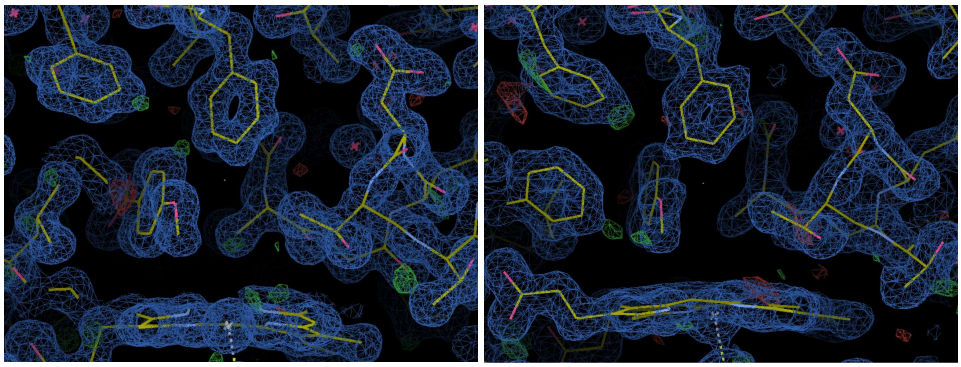

100 K 150 K

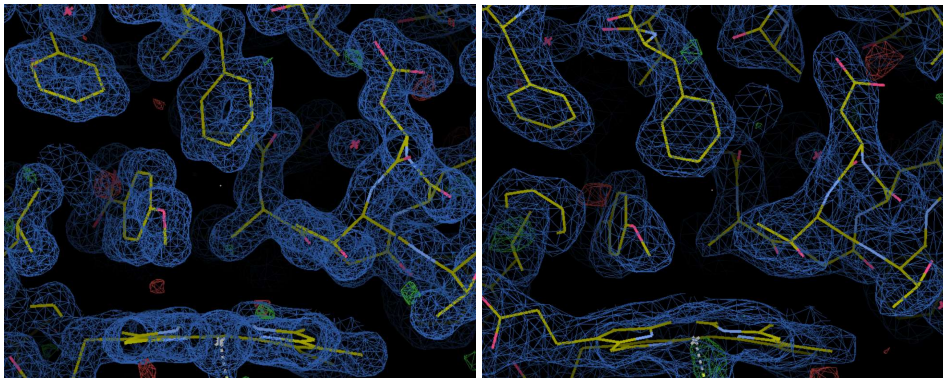

200 K 300 K

Figure S35a. The active site of the crystal structure of 4-methoxybenzoic acid-bound CYP199A4 at 100, 150, 200 and 300 K. The $2mF_o$-DF_c electron density map is shown as blue mesh (1 σ) and the mF_o-DF_c difference map is shown as red/green mesh (±3 σ).

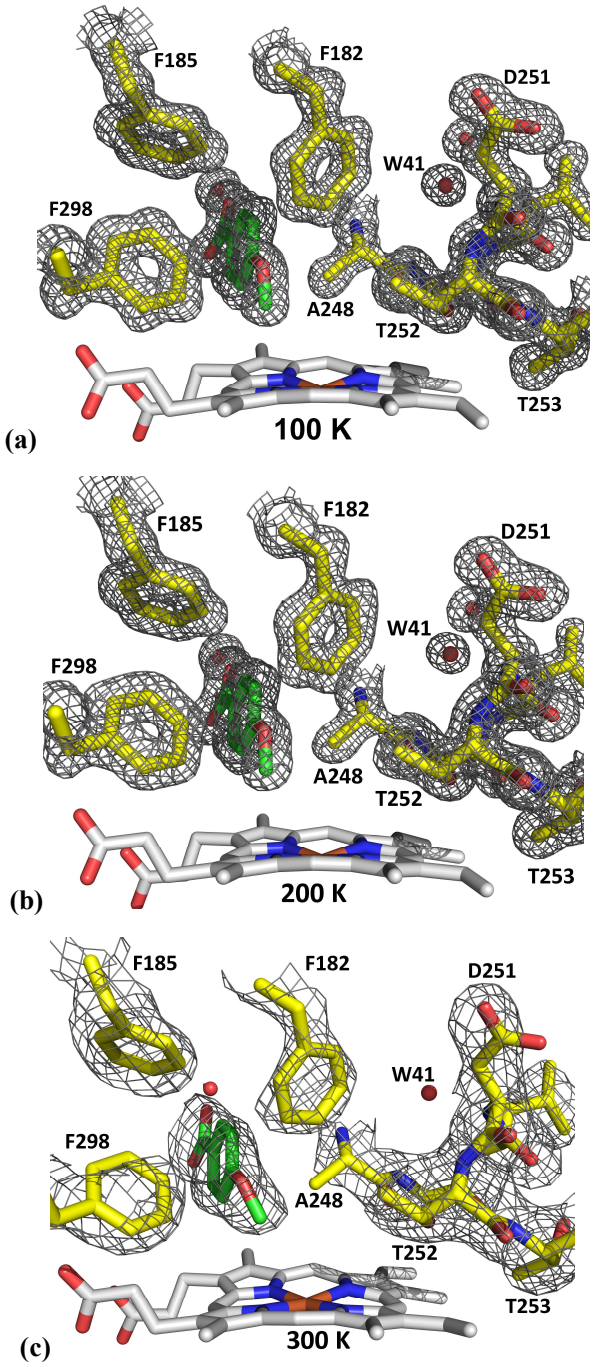

Figure S35b. The active site of the crystal structures of 4-methoxybenzoic acid-bound CYP199A4 at **(a)** 100 K, **(b)** 200 K and **(c)** 300 K. A $2mF_o$-DF_c composite omit map is shown as grey mesh contoured at 1.0 σ (1.5 A carve).

At 300 K, the electron density for the D251 side chain is poorer. There is no electron density missing for the F182 side chain.

Comparison of the new and previously determined crystal structures of 4-methoxybenzoic acid-bound CYP199A4 at 100 K

The structure of 4-methoxybenzoic acid-bound CYP199A4 was previously determined at 100 K (PDB code: 4DO1). The resolution of this previously reported structure is 2.00 Å.

The new 100 K structure was determined at significantly higher resolution (1.26-Å resolution) and is consistent with the previously determined structure. In both structures, the D251 side chain points out of the active site into the solvent channel. The Fe-S bond lengths are similar in both structures (2.40 and 2.36 Å).

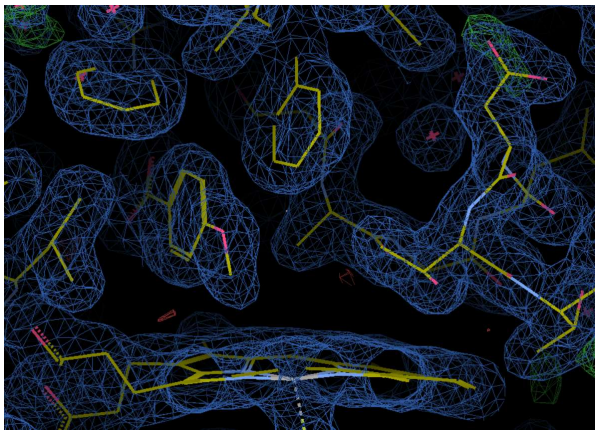

Previously solved structure (PDB code: 4DO1; 2.00 Å resolution)

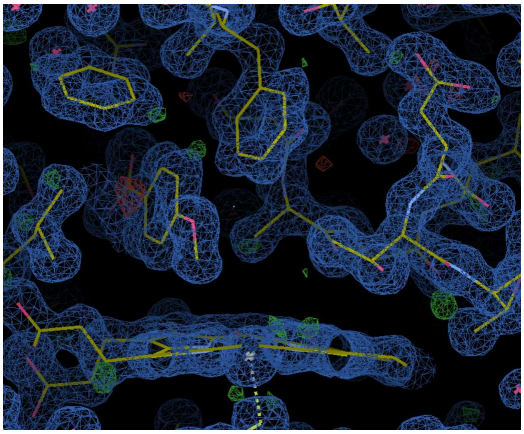

New structure (1.26-Å resolution)

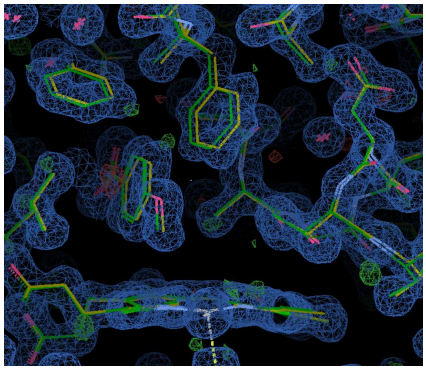

Above: Overlaying the new and previously determined structures (yellow and green sticks) demonstrates that the two structures are similar.

Figure S36. Comparison of the new and previously determined crystal structures of 4-methoxybenzoic acid-bound CYP199A4 at 100 K.

Table S19. Table of occupancy data for the crystal structures of CYP199A4 bound to 4-methoxybenzoic acid determined at 100 K

	Occupancy (%)	
	Previously solved structure (4DO1)	**New 100 K structure (9DOE)**
Heme-bound aqua ligand	Not present	Not present
D251 conformation pointing into active site	Not present	Not present
D251 conformation pointing out of active site (into water channel)	100%	100%

Comparison of the crystal structures of WT CYP199A4 bound to 4-methoxybenzoic acid at 100 K solved under different conditions (tetramer *vs* monomer)

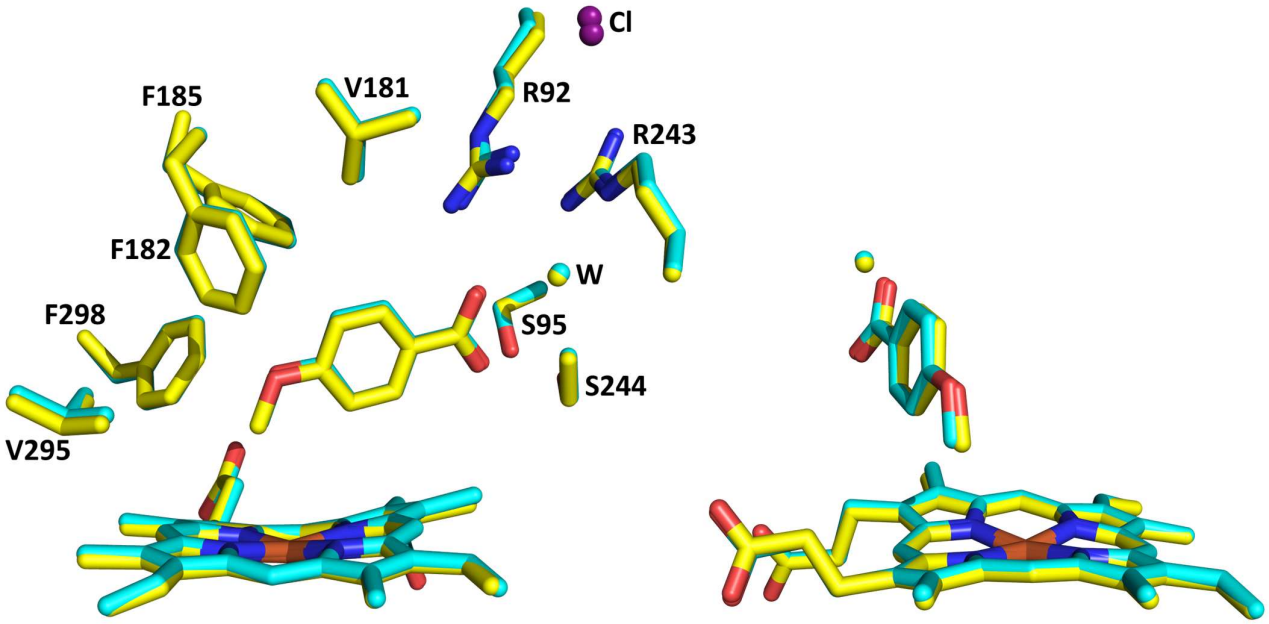

Figure S37. Comparison of the 100 K crystal structures of WT CYP199A4 bound to 4-methoxybenzoic acid solved under different conditions. The previously solved tetrameric crystal structure (PDB code: 4DO1, chain A) is shown in cyan. In yellow is the monomeric structure. The active site and position of the 4-methoxybenzoic acid substrate is highly similar in both crystal structures.

Table S20. Key distances in the high-resolution (monomeric) crystal structure of WT CYP199A4 bound to 4-methoxybenzoic acid

Distance (Å)	
Fe - C_{01}	3.9
Fe - O_{02}	5.1
Angle (˚)	
Dihedral (C_{04}-C_{03}-O_{02}-C_{01})	7.17
C_{03}-O_{02}-C_{01}	119.92

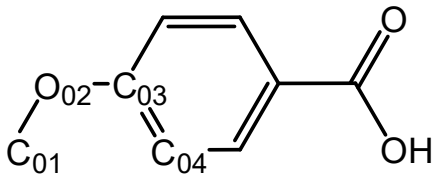

Refined occupancies of aspartate carboxylate groups in the variable-temperature crystal structures of wild-type CYP199A4 bound to 4-methoxybenzoic acid

To assess whether decarboxylation was occurring in these crystal structures, the D251 residue and four other aspartate residues were selected, and the occupancy of the side-chain carboxylate group was refined. The aspartate residues that were selected are all located on the surface of the protein.

The refined occupancy of certain aspartate carboxylate groups was lower in the 300 K structure than in the 100 K structure. This may indicate that some degree of radiation damage was occurring.

The selected aspartate residues occupy approximately the same position at each temperature. The images below showing the four overlaid structures demonstrate that the aspartate side chains have not moved significantly.

Table S21. Electron density maps of selected Asp/Glu residues in the three successive datasets at 100, 150 and 200 K.

The $2mF_o$-DF_c electron density map is shown contoured at 1.0 σ (blue mesh), and the mF_o-DF_c difference map is shown contoured at ± 3 σ (red and green mesh).

Aspartate residue	Position of the aspartate residue in the structures at 100 K, 150 K, 200 K, and 300 K	Aspartate residue	Position of the aspartate residue in the structures at 100 K, 150 K, 200 K, and 300 K
D251	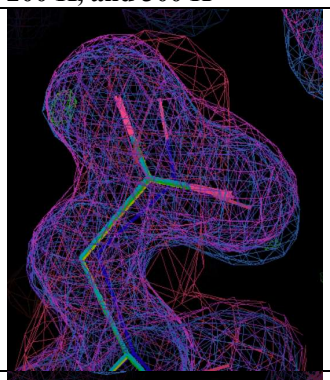	**D329**	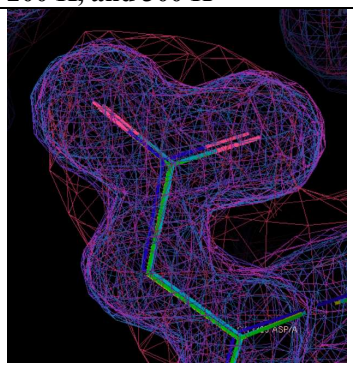
D277	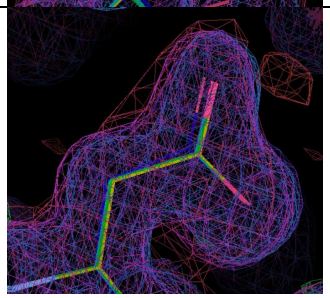	**D150**	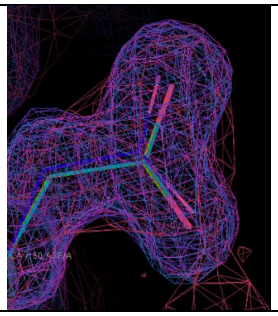
D383	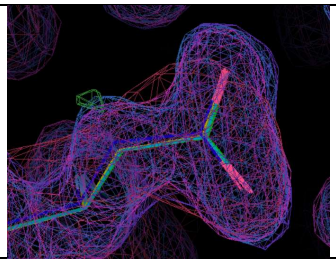		

Table S22 a. Refined occupancy of the D251 carboxylate in the crystal structures of wild-type CYP199A4 bound to 4-methoxybenzoic acid at 100 K, 150 K, 200 K and 300 K (increasing temperature series)

Dataset	Temperature (K)	Refined occupancy of the D251 carboxylate group (COO^-)
1	**100 K**	100%
2	**150 K**	84%
3	**200 K**	97%
4	**300 K**	65%

Table S22 b. Refined occupancy of the D277 carboxylate in the crystal structures of wild-type CYP199A4 bound to 4-methoxybenzoic acid at 100 K, 150 K, 200 K and 300 K (increasing temperature series)

Dataset	Temperature (K)	Refined occupancy of the D277 carboxylate group (COO^-)
1	**100 K**	100%
2	**150 K**	100%
3	**200 K**	100%
4	**300 K**	100%

Table S22 c. Refined occupancy of the D329 carboxylate in the crystal structures of wild-type CYP199A4 bound to 4-methoxybenzoic acid at 100 K, 150 K, 200 K and 300 K (increasing temperature series)

Dataset	Temperature (K)	Refined occupancy of the D329 carboxylate group (COO^-)
1	**100 K**	98%
2	**150 K**	79%
3	**200 K**	89%
4	**300 K**	100%

Table S22 d. Refined occupancy of the D150 carboxylate in the crystal structures of wild-type CYP199A4 bound to 4-methoxybenzoic acid at 100 K, 150 K, 200 K and 300 K (increasing temperature series)

Dataset	Temperature (K)	Refined occupancy of the D150 carboxylate group (COO^-)
1	**100 K**	91%
2	**150 K**	88%
3	**200 K**	87%
4	**300 K**	73%

Table S22 e. Refined occupancy of the D383 carboxylate in the crystal structures of wild-type CYP199A4 bound to 4-methoxybenzoic acid at 100 K, 150 K, 200 K and 300 K (increasing temperature series)

Dataset	Temperature (K)	Refined occupancy of the D383 carboxylate group (COO^-)
1	**100 K**	93%
2	**150 K**	100%
3	**200 K**	87%
4	**300 K**	86%

A248 does not move in the crystal structures of CYP199A4 bound to 4-methoxybenzoic acid at 100 K, 150 K and 200 K

When 4-methoxybenzoic acid binds to CYP199A4, it completely expels the heme-bound aqua ligand. The substrate and the A248 residue fail to move as the temperature of a crystal of 4-methoxybenozic acid-bound CYP199A4 is raised.

This suggests that the movement of A248 and the substrate observed in other structures is caused by the gradual disappearance of the heme-bound aqua ligand.

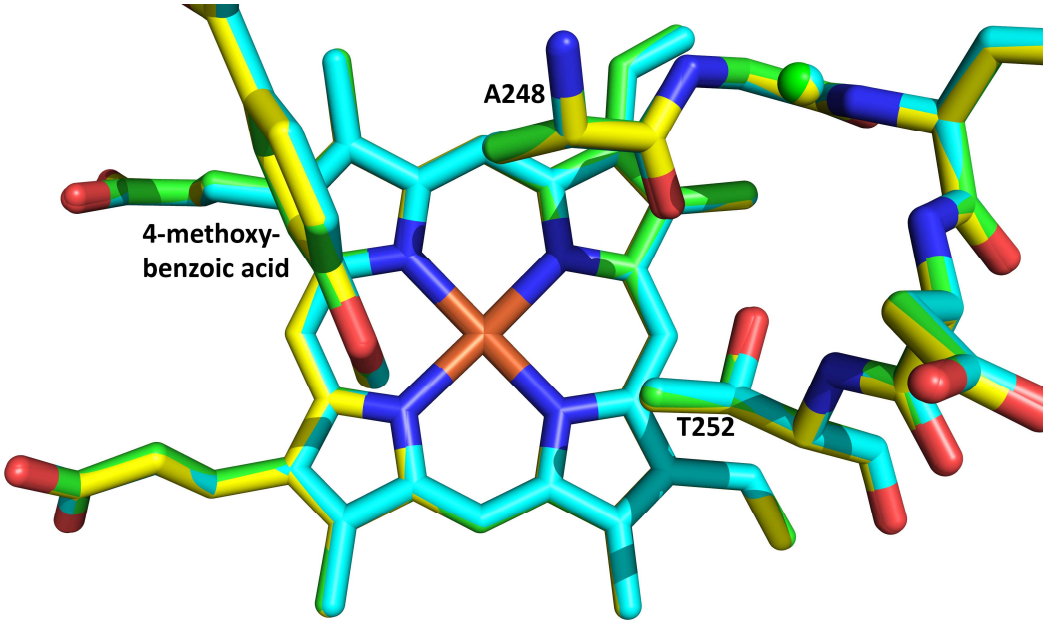

Figure S38. The overlaid crystal structures of CYP199A4 bound to 4-methoxybenzoic acid at 100 K (cyan), 150 K (green) and 200 K (yellow). No significant movement of A248 or the substrate occurs when the temperature is raised.

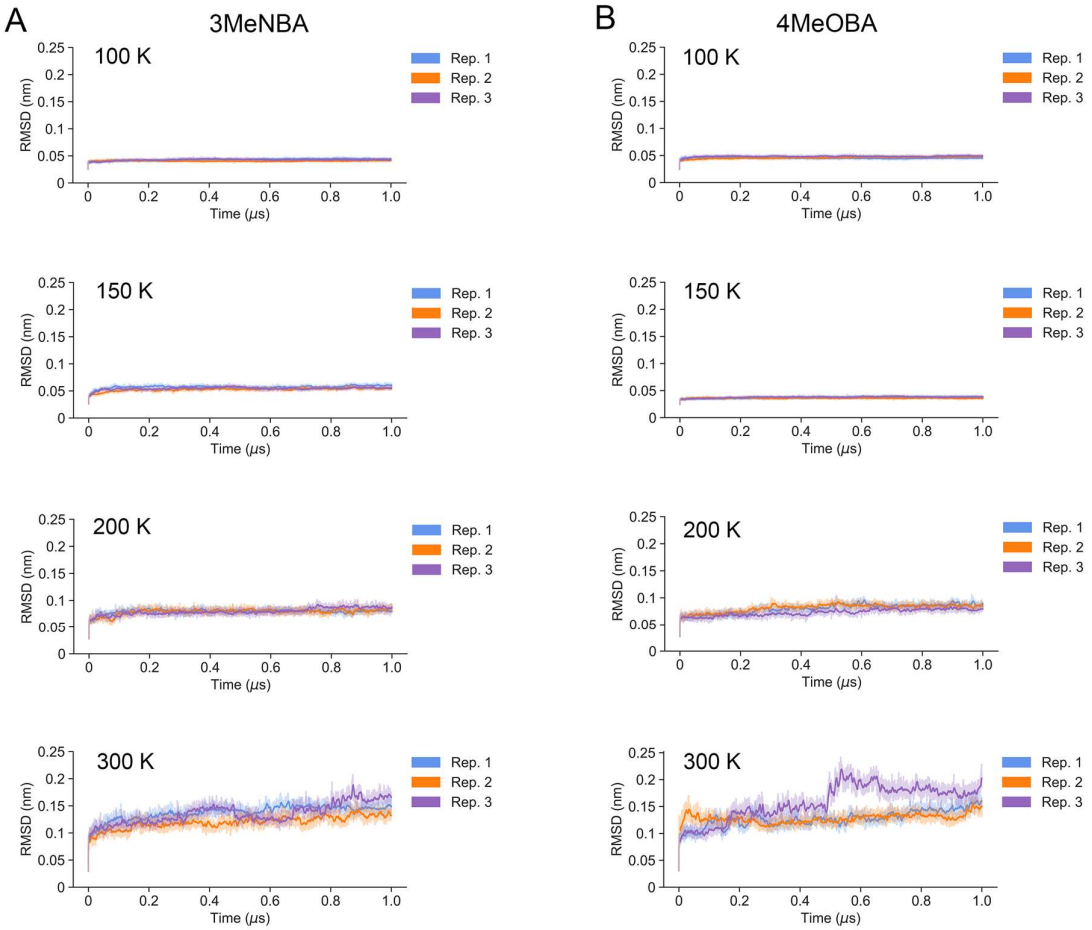

Figure S39. Plots depicting root mean-squared deviation (RMSD) of backbone heavy atoms for each replicate of the 3-methylaminobenzoic acid (3MeNBA; **A**) and 4-methoxybenzoic acid (4MeOBA; **B**) bound simulations at each temperature. The solid line is a the 5 ns rolling average.

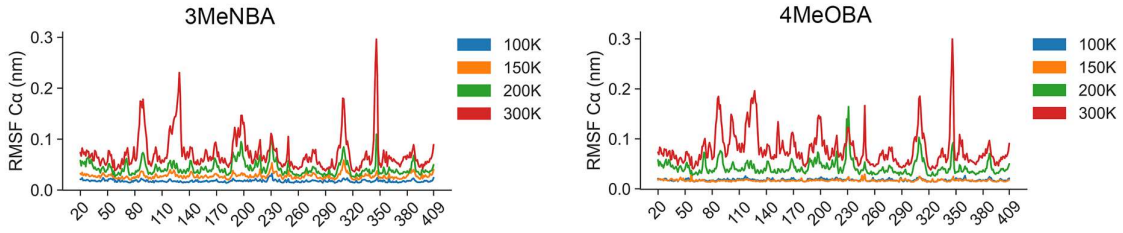

Figure S40. Average root mean-squared fluctuation (RMSF) of Cα-atoms for 3-methylaminobenzoic acid (3MeNBA) and 4-methoxybenzoic acid (4MeOBA) simulations over three replicate 1 μs simulations at each temperature range.

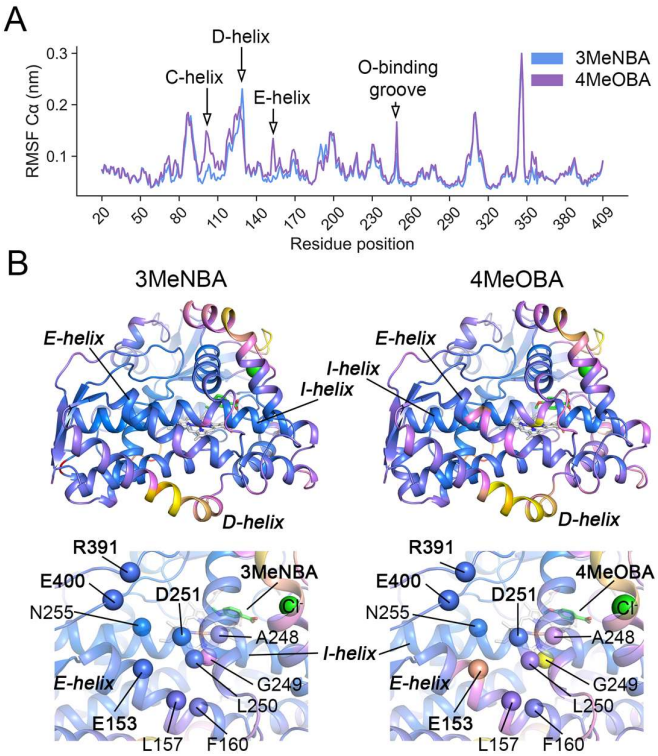

Figure S41. A) Average Cα-atom RMSF for 3-methylaminobenzoic acid (3MeNBA) and 4-methoxybenzoic acid (4MeOBA) simulations at 300 K, key regions of change are highlighted by downward arrows. B) (top) Average Cα-atom RMSF mapped to the starting coordinates structure (100 K) which shows dynamic variability between substrates, and (below) zoomed-in view of the residues involved in allosterically destabilising the E-helix. Dark blue residues are stable while yellow-orange-red residues increase in dynamics.

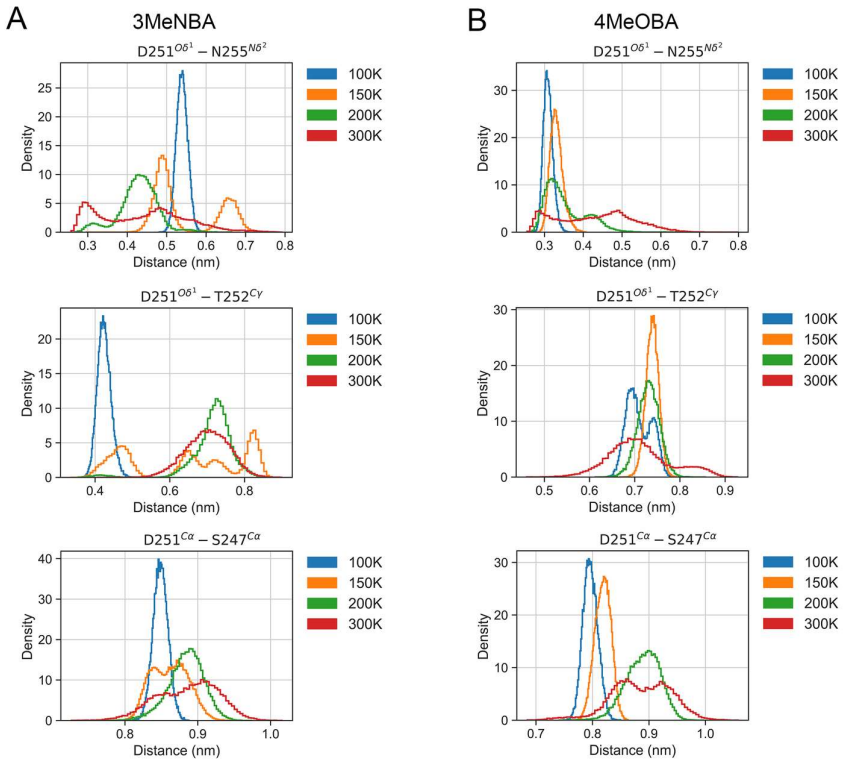

Figure S42. Density distribution of residue distances between D251-N255, D251-T252 and D251-S247 for 3-methylaminobenzoic acid (3MeNBA; **A**) and 4-methoxybenzoic acid (4MeOBA; **B**) simulations from three replicate 1 μs simulations at each temperature range.

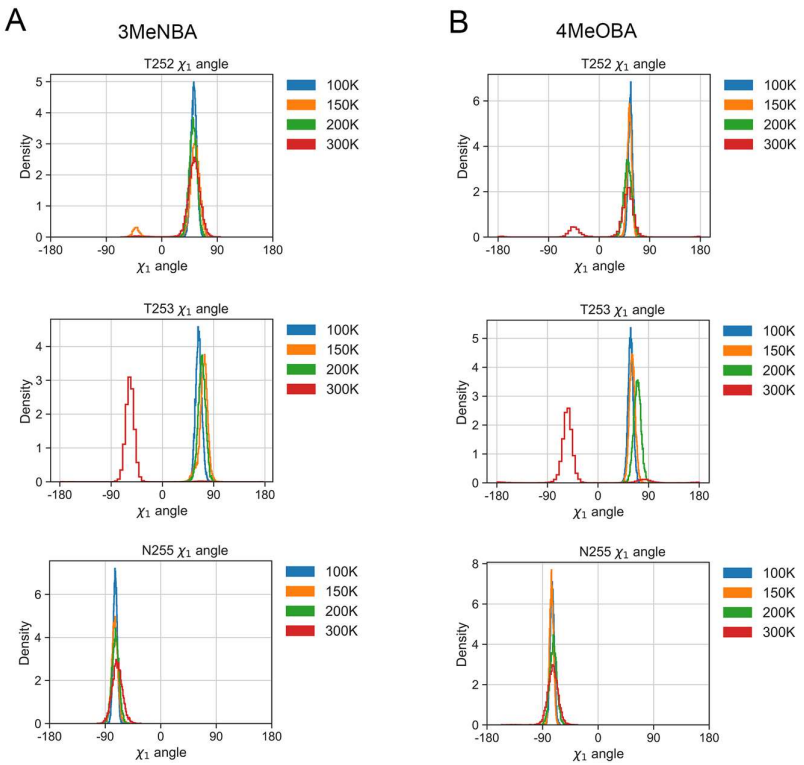

Figure S43. χ_1 sidechain dihedral angle density distribution of residues T252 (top), T253 (middle) and N255 (bottom) for 3-methylaminobenzoic acid (3MeNBA; **A**) and 4-methoxybenzoic acid (4MeOBA; **B**) simulations from three replicate 1 μs simulations at each temperature range.

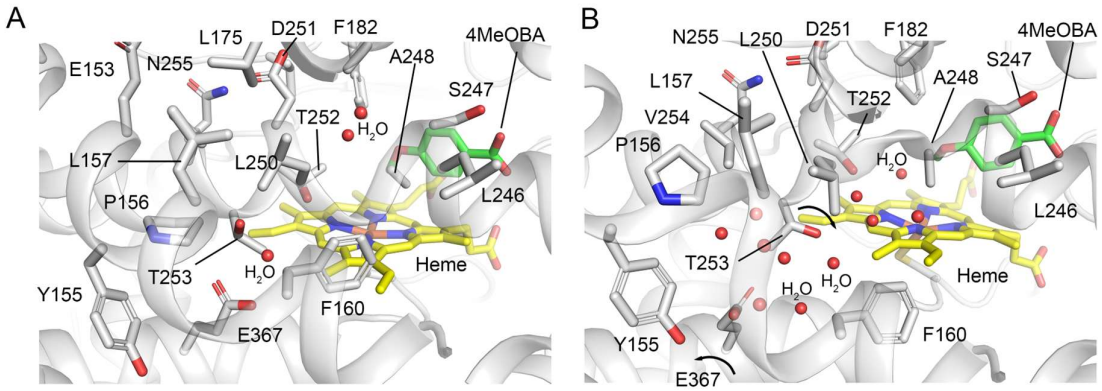

Figure S44. Simulation snapshots showing the solvent channel that passes above the D-helix and into the active site. A) The initial starting coordinates of the 4-methoxybenzoic acid (4MeOBA) structure are presented, showing two water molecules positioned in the oxygen-binding groove and the hydrogen bonding network between T253, a water and E367. B) A snapshot from a 300 K 4MeOBA simulation showing allosteric changes resulting in formation of the novel solvent channel enabling flux from the active site to the protein surface; not all water molecules are shown for clarity. Note the flipped conformations of T253 and E367, as well as the disorder of the oxygen-binding groove.

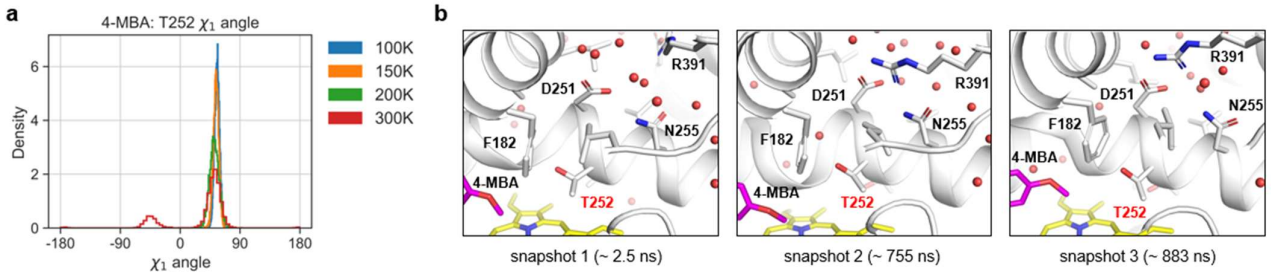

Figure S45. The dynamics of the T252 side chain in 4-methoxybenzoic acid (4-MBA) simulations. a) χ_1 of T252 sidechain across triplicate 1 μs simulations at 100 K, 150 K, 200 K and 300 K. b) Representative snapshots of T252 in the 'flipped' conformations across the duration of a 1 μs simulation and corresponding D251-R391 interactions. Sidechains are shown as sticks and water molecules are shown as red spheres.

Water network connected to D251 in the CYP199A4 crystal structures with 4-methoxybenzoic acid and 3-methylaminobenzoic acid bound

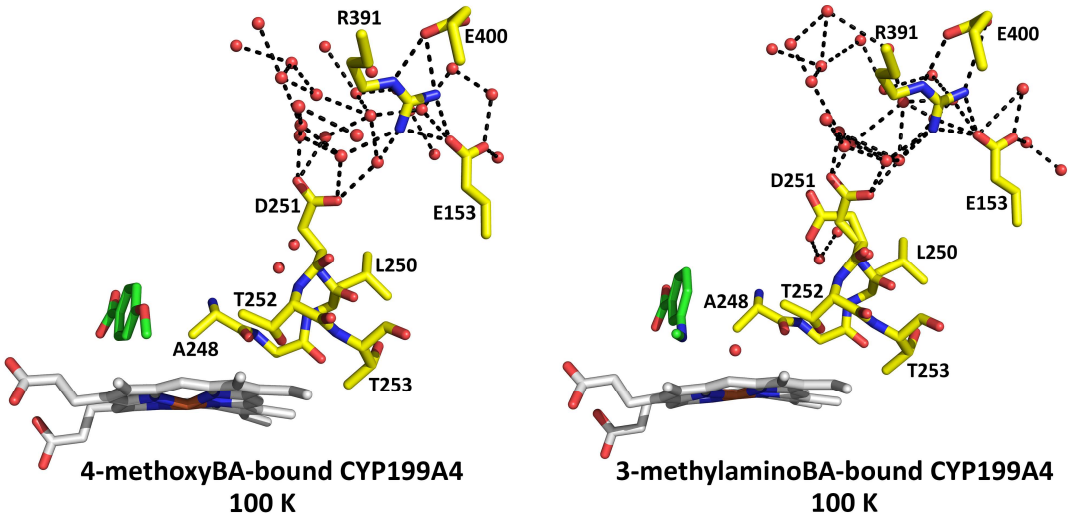

Figure S46a. The water network connected to D251 in the 100 K crystal structures of CYP199A4 with 4-methoxybenzoic acid and 3-methylaminobenzoic acid bound.

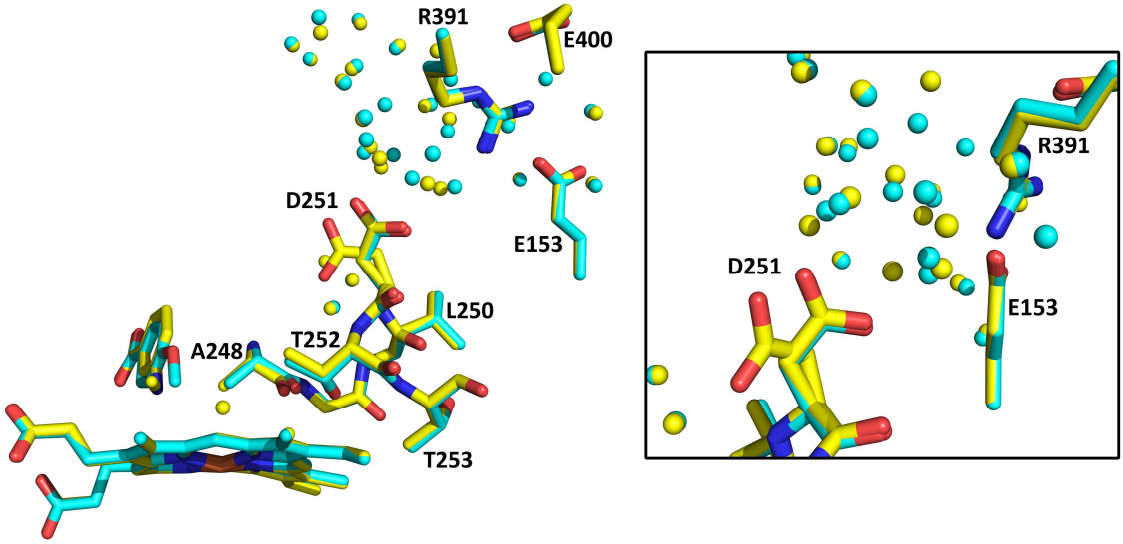

Figure S46b. The overlaid 100 K crystal structures of CYP199A4 bound to 4-methoxybenzoic acid (cyan) and 3-methylaminobenzoic acid (yellow), demonstrating that the water molecules in the network connected to D251 occupy different positions in the two structures.

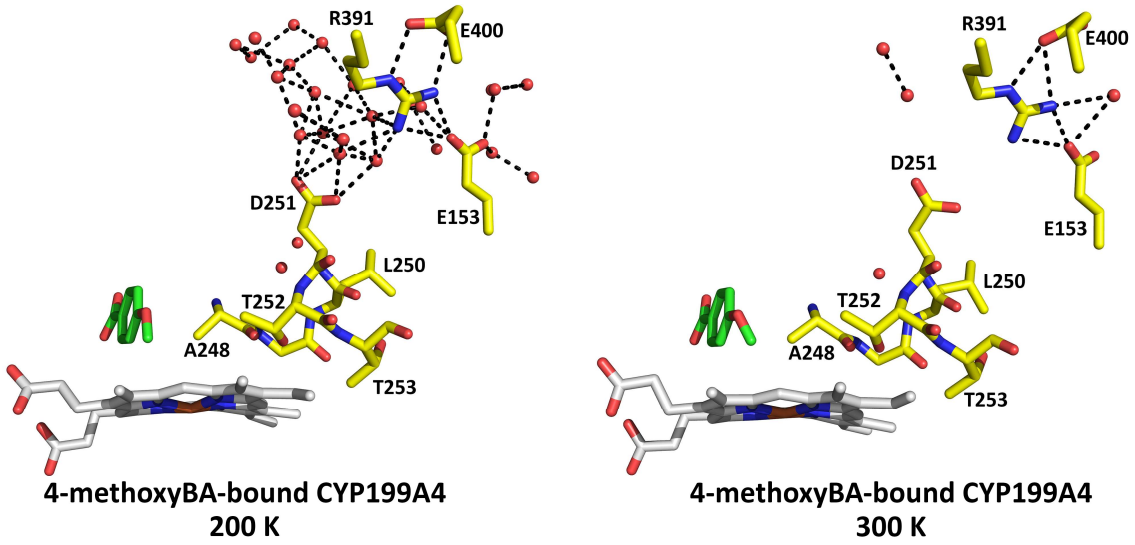

Figure S46c. A comparison of the water networks connected to the D251 residue in the 200 K and 300 K 4-methoxybenzoic acid-bound CYP199A4 crystal structures.

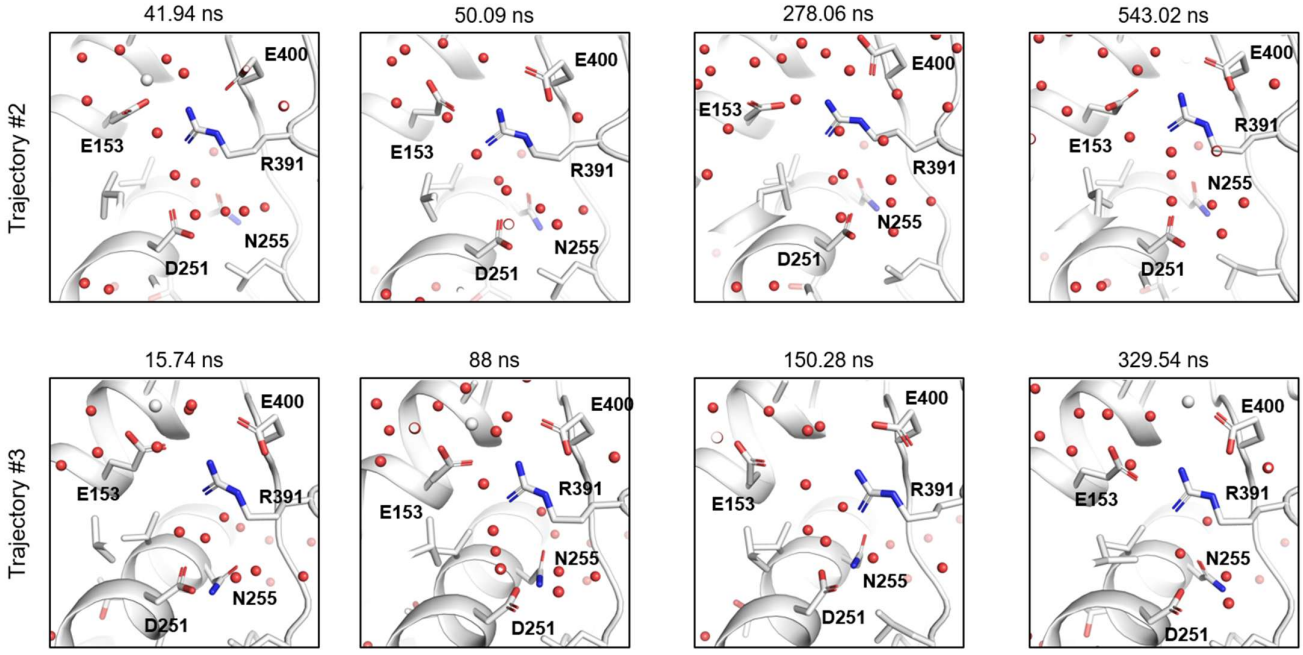

Figure S47. Representative snapshots of the E153-R391-E400 salt bridge network sampled across frames in trajectories two (top) and three (bottom) of the 4-methoxybenzoic acid MD simulations. Residues E153, D251, R391 and E400, and N255, are labelled in bold font; residue sidechains are shown as sticks and water molecules are shown as red spheres.

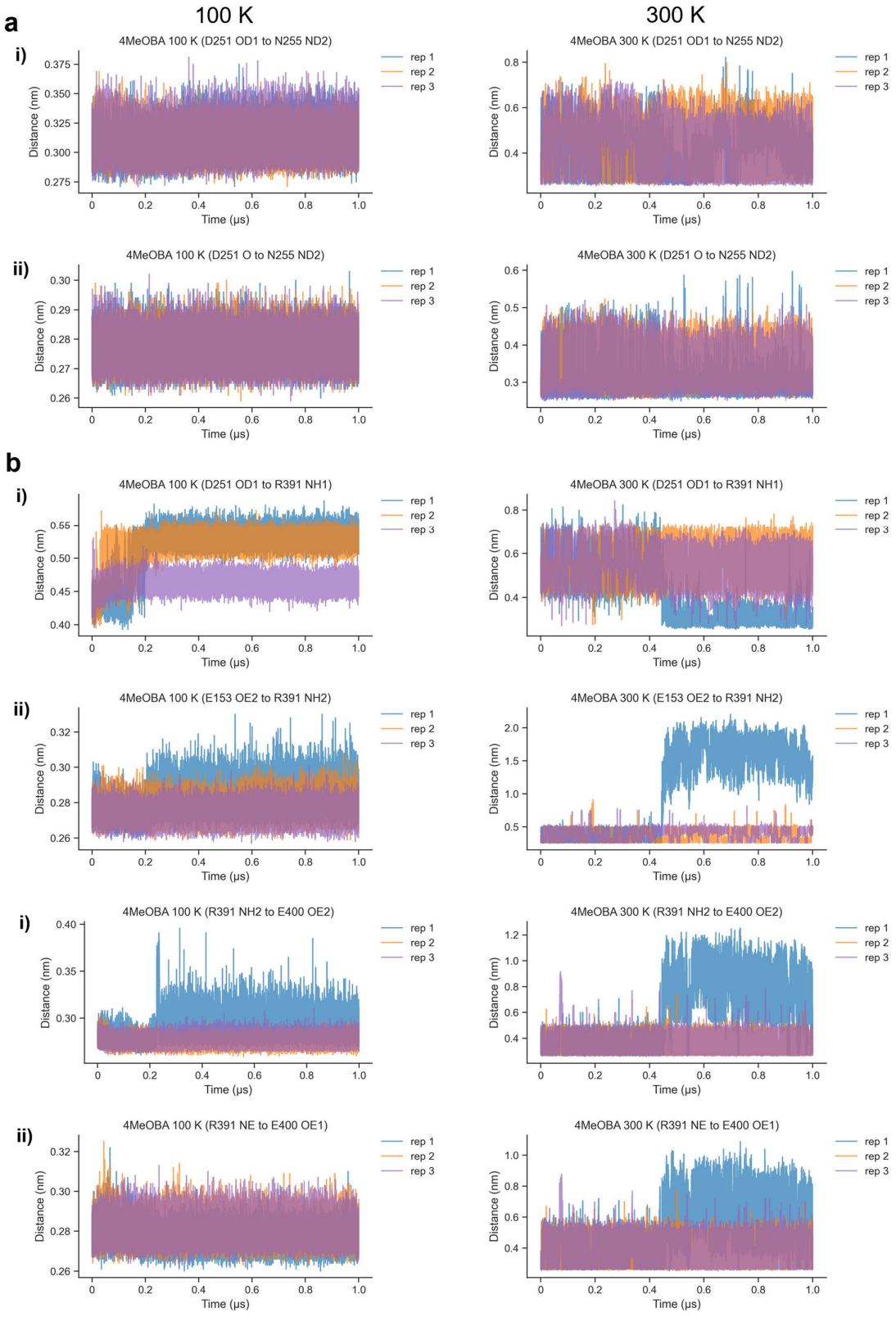

Figure S48a Distances between: (i) D251 sidechain Oδ^1 atom and N255 sidechain Nδ^2 atom, and (ii) D251 carbonyl O atom and N255 sidechain Nδ^2 atom in the 4-methoxybenzoic acid simulations at 100 K (left) and 300 K (right).

Figure S48b. Distances between: (i) D251 sidechain Oδ^1 atom and R391 sidechain NH^2 atom; (ii) E153 sidechain Oε^2 atom and R391 sidechain NH^2 atom; (iii) R391 sidechain NH^2 atom and E400 sidechain Oε^2 atom; (iv) R391 sidechain Nε atom and E400 sidechain Oε^1 atom, in the 4-methoxybenzoic acid simulations at 100 K (left) and 300 K (right).

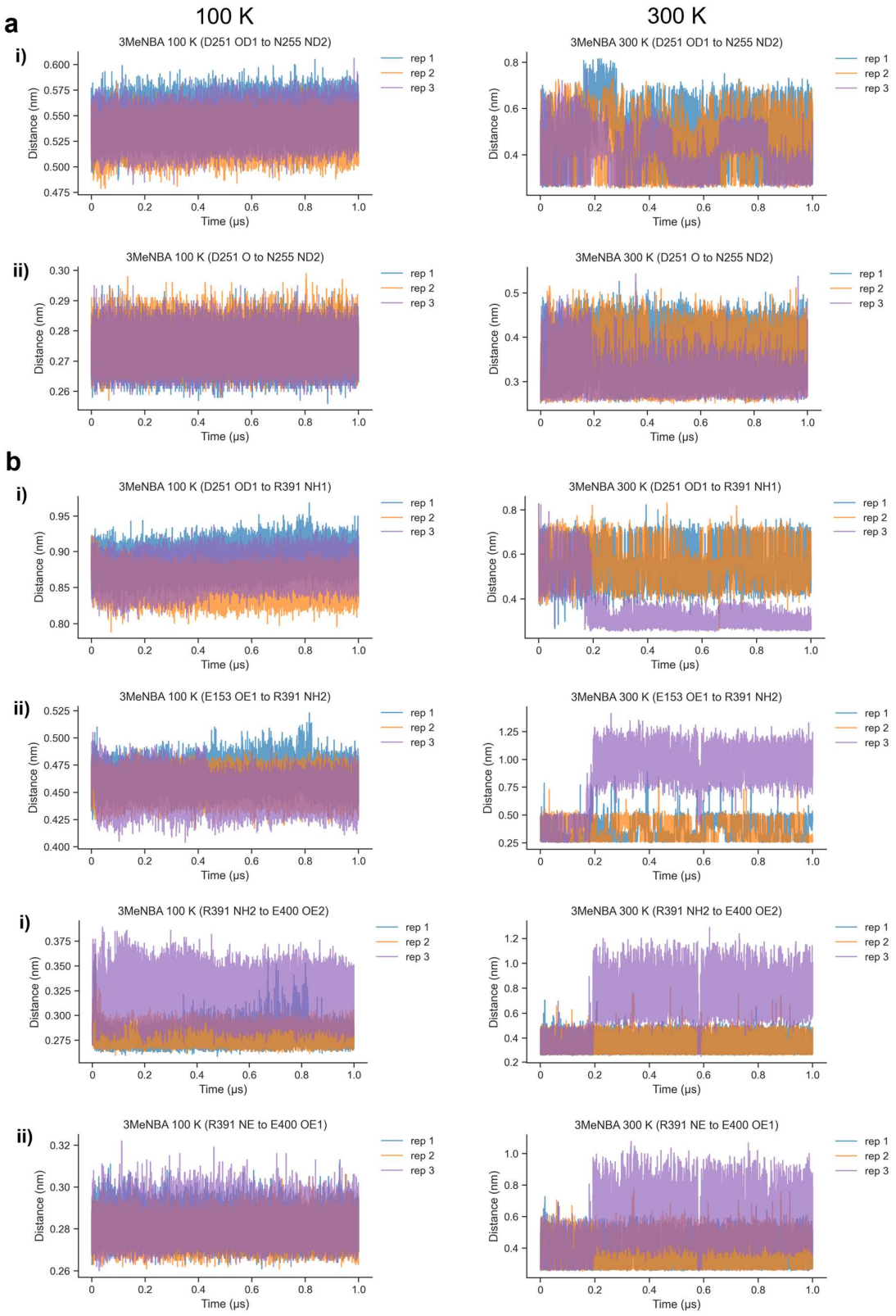

Figure S49a. Distances between: (i) D251 sidechain Oδ^1 atom and N255 sidechain Nδ^2 atom, and (ii) D251 carbonyl O atom and N255 sidechain Nδ^2 atom in the 3-methylaminobenzoic acid simulations at 100 K (left) and 300 K (right).

Figure S49b. Distances between: (i) D251 sidechain Oδ^1 atom and R391 sidechain NH^2 atom; (ii) E153 sidechain Oε^2 atom and R391 sidechain NH^2 atom; (iii) R391 sidechain NH^2 atom and E400 sidechain Oε^2 atom; (iv) R391 sidechain Nε atom and E400 sidechain Oε^1 atom, in the 3-methylaminobenzoic acid simulations at 100 K (left) and 300 K (right).

Table of coordinate errors

Table S23. Table of coordinate errors in the variable-temperature crystal structures of CYP199A4 bound to benzoic acid substrates

Crystal structure	Temperature (K)	Estimated coordinate error (Å)
CYP199A4 + 3-methylaminobenzoic acid (increasing temperature series)	100 K	0.13 Å
	150 K	0.14 Å
	200 K	0.19 Å
CYP199A4 + 3-methylaminobenzoic acid (decreasing temperature series)	200 K	0.20 Å
	150 K	0.21 Å
	100 K	0.20 Å
CYP199A4 + 4-methoxy-benzoic acid (increasing temperature series)	100 K	0.14 Å
	150 K	0.13 Å
	200 K	0.16 Å
	300 K	0.33 Å
CYP199A4 + 4-phenoxybenzoic acid (increasing temperature series)	100 K	0.19 Å
	150 K	0.17 Å
	200 K	0.19 Å

Reference List:

1. T. Coleman, J. E. Stok, M. N. Podgorski, J. B. Bruning, J. J. De Voss and S. G. Bell, Structural insights into the role of the acid-alcohol pair of residues required for dioxygen activation in cytochrome P450 enzymes, *JBIC Journal of Biological Inorganic Chemistry*, 2020, **25**, 583-596.
2. S. Nagano and T. L. Poulos, Crystallographic Study on the Dioxygen Complex of Wild-type and Mutant Cytochrome P450cam: Implications for the Dioxygen Activation Mechanism, *Journal of Biological Chemistry*, 2005, **280**, 31659-31663.
3. T. L. Poulos, Heme Enzyme Structure and Function, *Chemical Reviews*, 2014, **114**, 3919-3962.
4. T. L. Poulos and A. H. Follmer, Updating the Paradigm: Redox Partner Binding and Conformational Dynamics in Cytochromes P450, *Accounts of Chemical Research*, 2022, **55**, 373-380.
5. A. H. Follmer, S. Tripathi and T. L. Poulos, Ligand and Redox Partner Binding Generates a New Conformational State in Cytochrome P450cam (CYP101A1), *Journal of the American Chemical Society*, 2019, **141**, 2678-2683.
6. I. Ugur and P. Chandrasekhar, Proton relay network in P450cam formed upon docking of putidaredoxin, *Proteins: Structure, Function, and Bioinformatics*, 2020, **88**, 558-572.
7. M. N. Podgorski, A. B. Keto, T. Coleman, J. B. Bruning, J. J. De Voss, E. H. Krenske and S. G. Bell, The Oxidation of Oxygen and Sulfur-Containing Heterocycles by Cytochrome P450 Enzymes, *Chemistry – A European Journal*, 2023, DOI: https://doi.org/10.1002/chem.202301371, e202301371.
8. M. N. Podgorski, T. Coleman, P. D. Giang, C. R. Wang, J. B. Bruning, P. V. Bernhardt, J. J. De Voss and S. G. Bell, To Be, or Not to Be, an Inhibitor: A Comparison of Azole Interactions with and Oxidation by a Cytochrome P450 Enzyme, *Inorganic Chemistry*, 2022, **61**, 236-245.
9. M. N. Podgorski, T. Coleman, R. R. Chao, J. J. De Voss, J. B. Bruning and S. G. Bell, Investigation of the requirements for efficient and selective cytochrome P450 monooxygenase catalysis across different reactions, *Journal of Inorganic Biochemistry*, 2020, **203**, 110913.
10. S. G. Bell, W. Yang, A. B. H. Tan, R. Zhou, E. O. D. Johnson, A. Zhang, W. Zhou, Z. Rao and L.-L. Wong, The crystal structures of 4-methoxybenzoate bound CYP199A2 and CYP199A4: structural changes on substrate binding and the identification of an anion binding site, *Dalton Transactions*, 2012, **41**, 8703-8714.
11. E. Garman, Radiation damage in macromolecular crystallography: what is it and why should we care?, *Acta Crystallographica Section D*, 2010, **66**, 339-351.
12. I. Schlichting, J. Berendzen, K. Chu, A. M. Stock, S. A. Maves, D. E. Benson, R. M. Sweet, D. Ringe, G. A. Petsko and S. G. Sligar, The Catalytic Pathway of Cytochrome P450cam at Atomic Resolution, *Science*, 2000, **287**, 1615-1622.